

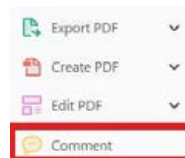
USING e-ANNOTATION TOOLS FOR ELECTRONIC PROOF CORRECTION

Required software to e-Annotate PDFs: [Adobe Acrobat Professional](#) or [Adobe Reader](#) (version 11 or above). (Note that this document uses screenshots from [Adobe Reader DC](#).)


The latest version of Acrobat Reader can be downloaded for free at: <http://get.adobe.com/reader/>

Once you have Acrobat Reader open on your computer, click on the [Comment](#) tab (right-hand panel or under the Tools menu).


This will open up a ribbon panel at the top of the document. Using a tool will place a comment in the right-hand panel. The tools you will use for annotating your proof are shown below:

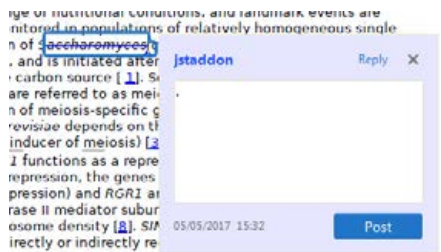


1. Replace (Ins) Tool – for replacing text.


 Strikes a line through text and opens up a text box where replacement text can be entered.

How to use it:

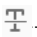
- Highlight a word or sentence.
- Click on .
- Type the replacement text into the blue box that appears.



2. Strikethrough (Del) Tool – for deleting text.

 Strikes a red line through text that is to be deleted.


How to use it:

- Highlight a word or sentence.
- Click on .
- The text will be struck out in red.



experimental data if available. For ORFs to be had to meet all of the following criteria:


1. Small size (35–250 amino acids).
2. Absence of similarity to known proteins.
3. Absence of functional data which could not be the real overlapping gene.
4. Greater than 25% overlap at the N-terminus terminus with another coding feature; over both ends; or ORF containing a tRNA.

3. Commenting Tool – for highlighting a section to be changed to bold or italic or for general comments.


 Use these 2 tools to highlight the text where a comment is then made.

How to use it:


- Click on .
- Click and drag over the text you need to highlight for the comment you will add.
- Click on .
- Click close to the text you just highlighted.
- Type any instructions regarding the text to be altered into the box that appears.




4. Insert Tool – for inserting missing text at specific points in the text.


 Marks an insertion point in the text and opens up a text box where comments can be entered.

How to use it:


- Click on .
- Click at the point in the proof where the comment should be inserted.
- Type the comment into the box that appears.



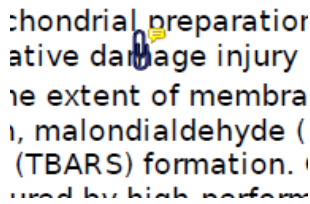
5. Attach File Tool – for inserting large amounts of text or replacement figures.

 Inserts an icon linking to the attached file in the appropriate place in the text.


How to use it:

- Click on  .
- Click on the proof to where you'd like the attached file to be linked.
- Select the file to be attached from your computer or network.
- Select the colour and type of icon that will appear in the proof. Click OK.


The attachment appears in the right-hand panel.

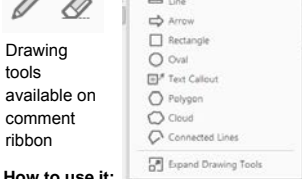
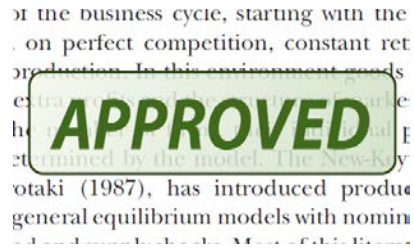


6. Add stamp Tool – for approving a proof if no corrections are required.

 Inserts a selected stamp onto an appropriate place in the proof.

How to use it:

- Click on  .
- Select the stamp you want to use. (The [Approved](#) stamp is usually available directly in the menu that appears. Others are shown under *Dynamic, Sign Here, Standard Business*).
- Fill in any details and then click on the proof where you'd like the stamp to appear. (Where a proof is to be approved as it is, this would normally be on the first page).

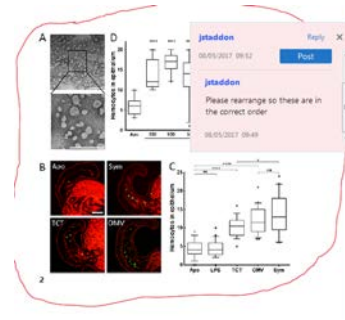


How to use it:

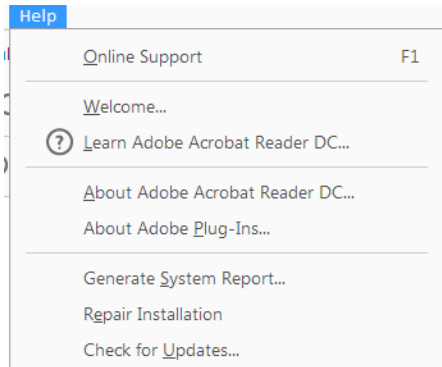
- Click on one of the shapes in the [Drawing Markups](#) section.
- Click on the proof at the relevant point and draw the selected shape with the cursor.
- To add a comment to the drawn shape, right-click on shape and select *Open Pop-up Note*.
- Type any text in the red box that appears.

7. Drawing Markups Tools – for drawing shapes, lines, and freeform annotations on proofs and commenting on these marks.

Allows shapes, lines, and freeform annotations to be drawn on proofs and for comments to be made on these marks.



For further information on how to annotate proofs, click on the [Help](#) menu to reveal a list of further options:



Author Query Form

Journal: BRE

Article: 12266

Dear Author,

During the copyediting of your manuscript the following queries arose.

Please refer to the query reference callout numbers in the page proofs and respond to each by marking the necessary comments using the PDF annotation tools.


Please remember illegible or unclear comments and corrections may delay publication.

Many thanks for your assistance.

Query reference	Query	Remarks
1	AUTHOR: Kindly check and approve the edits made in article title.	
2	AUTHOR: Please supply a short title of up to 40 characters that will be used as the running head.	
3	AUTHOR: Please confirm that given names (red) and surnames/family names (green) have been identified correctly.	
4	AUTHOR: Please provide an appropriate table footnote to explain the bold letters in Table 2.	
5	AUTHOR: Morhiak and Leroy, 2012 has been changed to Mohriak and Leroy, 2013 so that this citation matches the Reference List. Please confirm that this is correct.	
6	AUTHOR: Please provide the volume number for reference Berglund et al. (1986).	
7	AUTHOR: Please provide the volume number for reference Dabrio (1990).	
8	AUTHOR: Please provide the page range for reference Jakobsson et al. (2012).	
9	AUTHOR: Nøhr-Hansen (1993) has not been cited in the text. Please indicate where it should be cited; or delete from the Reference List.	
10	AUTHOR: Please provide the volume number for reference Surlyk (1989).	

Funding Info Query Form

Please confirm that the funding sponsor list below was correctly extracted from your article: that it includes all funders and that the text has been matched to the correct FundRef Registry organization names. If a name was not found in the FundRef registry, it may not be the canonical name form, it may be a program name rather than an organization name, or it may be an organization not yet included in FundRef Registry. If you know of another name form or a parent organization name for a “not found” item on this list below, please share that information.

FundRef name	FundRef Organization Name (Country)
ARCEX project (Research Center for Arctic Petroleum Exploration) 	

Unravelling key controls on the rift climax to post-rift fill of marine rift basins: insights from 3D seismic analysis of the Lower Cretaceous of the Hammerfest Basin, SW Barents Sea

Dora Marín,* Alejandro Escalona,* Sten-Andreas Grundvåg,† Snorre Olaussen,‡ Sara Sandvik§ and Kasia K. Śliwińska¶

*Department of Petroleum Engineering, University of Stavanger, Stavanger, Norway

†Department of Geosciences, University of Tromsø – The Arctic University of Norway, Tromsø, Norway

‡Department of Arctic Geology, UNIS the University Centre in Svalbard, Longyearbyen, Norway

§Exploration geologist at Lundin, Oslo, Norway

¶Geological Survey of Denmark and Greenland (GEUS), Copenhagen K, Denmark

ABSTRACT

In this study, we investigate key factors controlling the rift climax to post-rift marine basin fill. We use two- and three-dimensional seismic data in combination with sedimentological core descriptions from the Hammerfest Basin, south-western Barents Sea to characterize and analyse the tectonostratigraphy and seismic facies of the Lower Cretaceous succession. Based on our biostratigraphic analyses, the investigated seismic facies are correlated to 5–10 million year duration sequences that make up the stratigraphic framework of the basin fill. The seismic facies suggest the basin fill was deposited in shallow to deep-marine conditions. During rift climax in Volgian/Berriasian to Barremian times, a fully linked fault array controlled the formation of slope systems consisting of gravity flow deposits along the southern margin of the basin. Renewed uplift of the Loppa High north of the basin provided coarse-grained sediments for fan deltas and shorelines that developed along the northern basin margin. During the early to middle late Aptian, the input of coarse-grained sediments occurred mainly in the NW and SW corners of the basin, reflecting renewed uplift-induced topography in the western flank of the Loppa High and along the western Finnmark Platform. The lower Albian part of the basin fill is interpreted as a post-rift succession, where the remnant topography associated with the Finnmark Platform continued to provide sediments to prograding fan deltas and adjacent shorelines. During the Albian, a series of faults were reactivated in the northern part of the basin, and footwall wedges comprising various gravity flow deposits occur along these faults. During the latest Albian to Cenomanian, the south-eastern part of the Loppa High was flooded by a rise in eustatic sea-level and differential subsidence. However, the western part of the high remained exposed and acted as a sediment source for a shelf-margin system prograding towards the SE. It is concluded that the rift climax succession is controlled by: along strike variability of throw and steps of the main bounding faults; the diachronous movement of the faults; and the nature of the feeder system. The evolution of the post-rift succession may be controlled by rifting in adjacent basins which preferentially renew sources of sediments; local reactivation of faults; and local remnant topography of the basin flanks. We suggest that existing tectonostratigraphic models for rift basins should be updated, to incorporate a more regional perspective and integrating variables such as the influence of adjacent rift systems.

Correspondence: Dora Marín, Department of Petroleum Engineering, University of Stavanger, NO-4036 Stavanger, Norway.
E-mail: dora.l.restrepo@uis.no



B R E Journal Code	12266 Manuscript No.	WILEY	
		Dispatch: 27.9.17	CE: Hari Hara Sudan K PE: Maheswari S.
		No. of pages: 26	

INTRODUCTION

Marine rift basins are commonly prolific for hydrocarbons because of their large preservation potential of all the elements in a potential petroleum system (e.g. seal, reservoir and source rocks) (Gawthorpe & Leeder, 2000). The prediction of facies related to source rocks, and particular reservoir rocks and their lateral and vertical continuity is challenging, because depositional environments in rift basins may range from continental to deep-marine environments due to the contrast in topography along the faults (Ravnås & Steel, 1998). The infill of marine rift basins is controlled by several variables: climate, eustatic sea-level, subsidence, drainage evolution, footwall lithology, nature of the feeder system (e.g. point source, multiple source or linear source), variability along the strike of the faults and basin physiography (Stow *et al.*, 1996; Ravnås & Steel, 1998; Allen & Densmore, 2000; Gawthorpe & Leeder, 2000; McArthur *et al.*, 2013; Sømme *et al.*, 2013; Elliott *et al.*, 2017). Some of these variables are determined by the evolution of fault propagation, which typically depends on the stage of the rift evolution (Cowie *et al.*, 2000; Gawthorpe & Leeder, 2000). A single rift phase is constituted by rift initiation and rift climax, followed by a post-rift phase (Prosser, 1993). The rift initiation is characterized by several small and isolated basins with low rates of subsidence as a result of strain being distributed along many minor faults (Prosser, 1993; Gupta *et al.*, 1998; Cowie *et al.*, 2000; Gawthorpe & Leeder, 2000). Rift climax is characterized by fully linked faults, where deformation is concentrated over the major faults (Gupta *et al.*, 1998; Cowie *et al.*, 2000; Gawthorpe & Leeder, 2000; Leppard & Gawthorpe, 2006). Subsidence commonly outpaces sedimentation, resulting in the deposition of deep-marine mudstones with localized coarse clastic wedges deposited close to the footwall area (Leppard & Gawthorpe, 2006). Coarse-grained sediments have been described at the base of the fault scarp in slope aprons, slumps and slides, talus and coarse-grained aggradational or progradational fan deltas (Surlyk, 1978, 1989; Stow *et al.*, 1996; Gawthorpe *et al.*, 1997; Leppard & Gawthorpe, 2006; Larsen *et al.*, 2010; Henstra *et al.*, 2016; Elliott *et al.*, 2017). Progradation tends to occur with low accommodation or high sediment supply or a combination of these factors (Gawthorpe & Leeder, 2000). The boundary between the syn-rift to post-rift stages can be diachronous and is marked by the end of the faulting and thermal contraction subsidence influence (Prosser, 1993; Nøttvedt *et al.*, 1995; Gabrielsen *et al.*, 2001; Zachariah *et al.*, 2009). The post-rift phase is usually divided into 1) an early post-rift phase, where wedge geometries are commonly developed associated with remnant topography inherited from the rift phase (Prosser, 1993; Nøttvedt *et al.*, 1995; Zachariah *et al.*, 2009) and 2) a late post-rift period, where the

continued erosion of the footwall crest leads to a reduction in the topographic highs which usually yields finer grain-size sediments (Prosser, 1993). Much effort has been made to understand the variables controlling the sedimentation in rift systems (e.g. Prosser, 1993; Nøttvedt *et al.*, 1995; Gupta *et al.*, 1998; Ravnås & Steel, 1998; Cowie *et al.*, 2000; Gawthorpe & Leeder, 2000; Gabrielsen *et al.*, 2001; Leppard & Gawthorpe, 2006; Zachariah *et al.*, 2009; McArthur *et al.*, 2013; Elliott *et al.*, 2017). In addition, tectonostratigraphic models have been developed for single rift systems (Gawthorpe & Leeder, 2000), and more recently updated to include multiphase rifts (Henstra *et al.*, 2017). However, variables such as the influence of adjacent rift systems in the post-rift evolution have been poorly documented.

The Hammerfest Basin is located in the south-western Barents Sea (Fig. 1). The basin experienced rifting during the Late Jurassic–Early Cretaceous times (Berglund *et al.*, 1986; Gabrielsen *et al.*, 1990; Faleide *et al.*, 1993), but did not evolve to break-up. Lower Cretaceous clastic wedges deposited during this rift event are considered a play model in the area (Seldal, 2005; NPD, 2017); oil and gas discoveries (e.g. wells 7120/2-3S, 7120/1-2) and rocks with reservoir potential (e.g. wells 7120/10-2, 7120/6-3S and 7122/2-1) have been found (Seldal, 2005; NPD, 2017). Previous studies in the Hammerfest Basin have analysed the Lower Cretaceous succession in isolation, and no systematic tectonostratigraphic framework has been built in order to map the temporal and spatial variations of the syn-rift to post-rift sequences. There are few published sedimentological descriptions of the wedges (see Sandvik, 2014 for core descriptions of wells 7120/1-2 and 7120/2-2 located in the north-western part of the basin). Neither their internal architecture, lateral variability nor their ages have been characterized for the entire basin. In addition, there are large uncertainties regarding their depositional environments. Some of the wedges have been described as shallow marine (wells 7120/1-2 and 7120/2-2) or fan deltas (well 7120/2-2), whereas others have been interpreted as distal turbidite systems (wells 7120/12-1 and 7120/10-1) (Knutsen *et al.*, 2000; Seldal, 2005; Sattar, 2008; Sandvik, 2014). This reflects the complex distribution of facies in marine rift basins.

Aim of the study

The main aims of this study are as follows: 1) to use tectonostratigraphy and characterization of seismic facies to understand the factors controlling the rift climax to post-rift basin fill. Particularly to investigate how rifting in adjacent basins may control the evolution of the post-rift succession; 2) to describe and interpret the stratigraphic architecture of the Lower Cretaceous succession of the Hammerfest Basin and variability in depositional

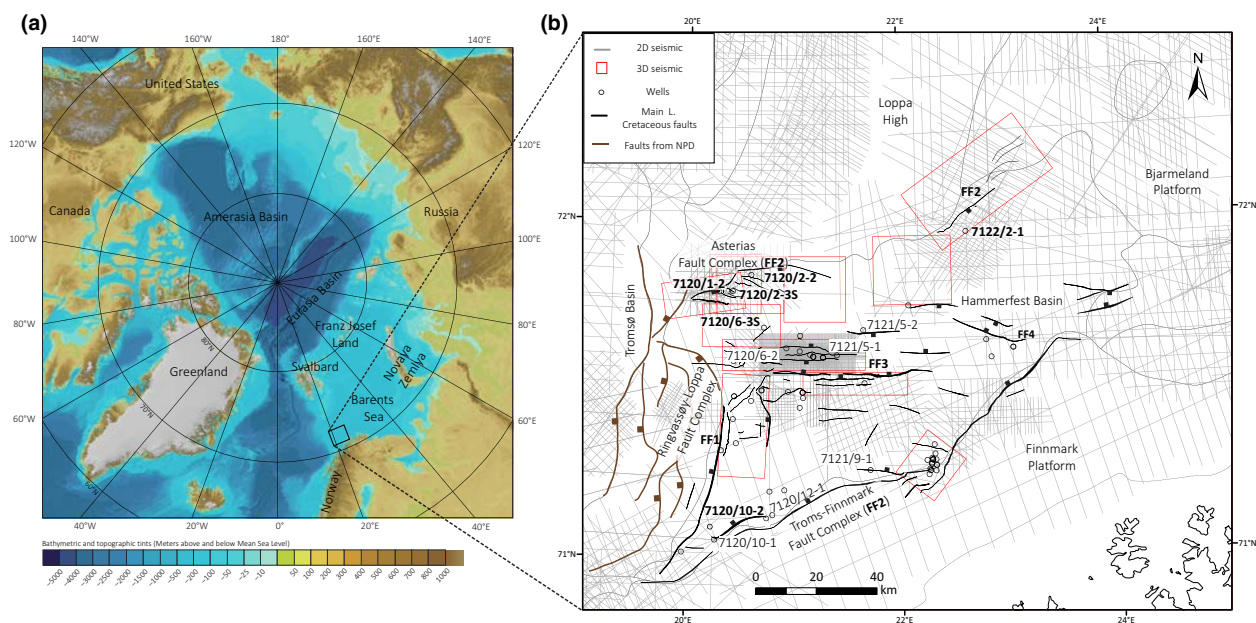


Fig. 1. (a) Bathymetric map of the Arctic Ocean (Jakobsson *et al.*, 2012); (b) location map with the geological elements of the study area, fault families and the data used in this study. Brown faults and well information from NPD (2017). Six wells with sedimentological core descriptions are indicated with bold text.

environments with respect to the recognized stages of rifting; and 3) to improve the age control of the seismic facies and correlate them within a basin wide stratigraphic framework (Marín *et al.*, 2017). This is achieved by combining two- and three-dimensional seismic data with wire line logs, core data and dinoflagellate cyst (dinocyst) biostratigraphy. Seismic facies analysis formed the basis for the sedimentological interpretations. Where available, well control and cored intervals aided our interpretations. The range of the seismic facies described here helps to elucidate the distribution and the origin of the Lower Cretaceous sandstones in the Hammerfest Basin and can be used for facies prediction in areas with challenging geophysical imaging (e.g. presalt section).

GEOLOGICAL SETTING

Tectonic framework

The Hammerfest Basin is a symmetric and elongated ENE–WSW-striking basin. The southern border towards the Finnmark Platform is defined by the Troms–Finnmark Fault Complex (TFFC), (Fig. 1) (Sund *et al.*, 1986; Gabrielsen *et al.*, 1990). The north-western boundary is marked by the Asterias Fault Complex (AFC), which separates the basin from the Loppa High. The western boundary with the Tromsø Basin is marked by the Ringvassøy–Loppa Fault Complex (RLFC), and the eastern boundary towards the Bjarmeland Platform is not faulted (Figs 1 and 2) (Gabrielsen *et al.*, 1990).

During the Late Jurassic to Early Cretaceous, the basin experienced extension (Berglund *et al.*, 1986; Gabrielsen *et al.*, 1990; Faleide *et al.*, 1993). Some of the faults formed in this event were conditioned by the structures of the Caledonian basement (Gabrielsen *et al.*, 1990; Doré, 1991). A gentle central high was formed during the Late Jurassic–Early Cretaceous in the western part of the basin, as a flexural rollover due to the activity of the AFC and TFFC (Fig. 2a) (Berglund *et al.*, 1986; Sund *et al.*, 1986; Gabrielsen *et al.*, 1990; Faleide *et al.*, 1993; Larsen *et al.*, 2002). The eastern part of the basin is interpreted as a sag basin, with a monocline in the north-eastern boundary with the Loppa High (Gabrielsen *et al.*, 1990). β -Factors of 1.8 or 3 have been calculated for the neighbouring Bjørnøya Basin (Clark *et al.*, 2014) and <1.3 for the Hammerfest Basin for the Late Jurassic to Early Cretaceous rift event (Leknes, 2008). A local compression during the earliest Cretaceous has been suggested for the AFC in the north-western part of the basin, forming a local high and along the TFFC (Fig. 2a) (Berglund *et al.*, 1986; Sund *et al.*, 1986; Gabrielsen *et al.*, 1990; Indrevær *et al.*, 2016). The compression has been interpreted as a result of strike slip movements (Berglund *et al.*, 1986; Sund *et al.*, 1986; Gabrielsen *et al.*, 1990) or as a localized inversion due to differential uplift of the Loppa High (Indrevær *et al.*, 2016). Moreover, three Cretaceous extensional phases (Berriasian–Valanginian, Hauterivian–Barremian and Aptian–Albian) have been interpreted for the adjacent Tromsø Basin (Faleide *et al.*, 1993). Faleide *et al.* (1993) described that the Kolmule Formation thins

COLOR

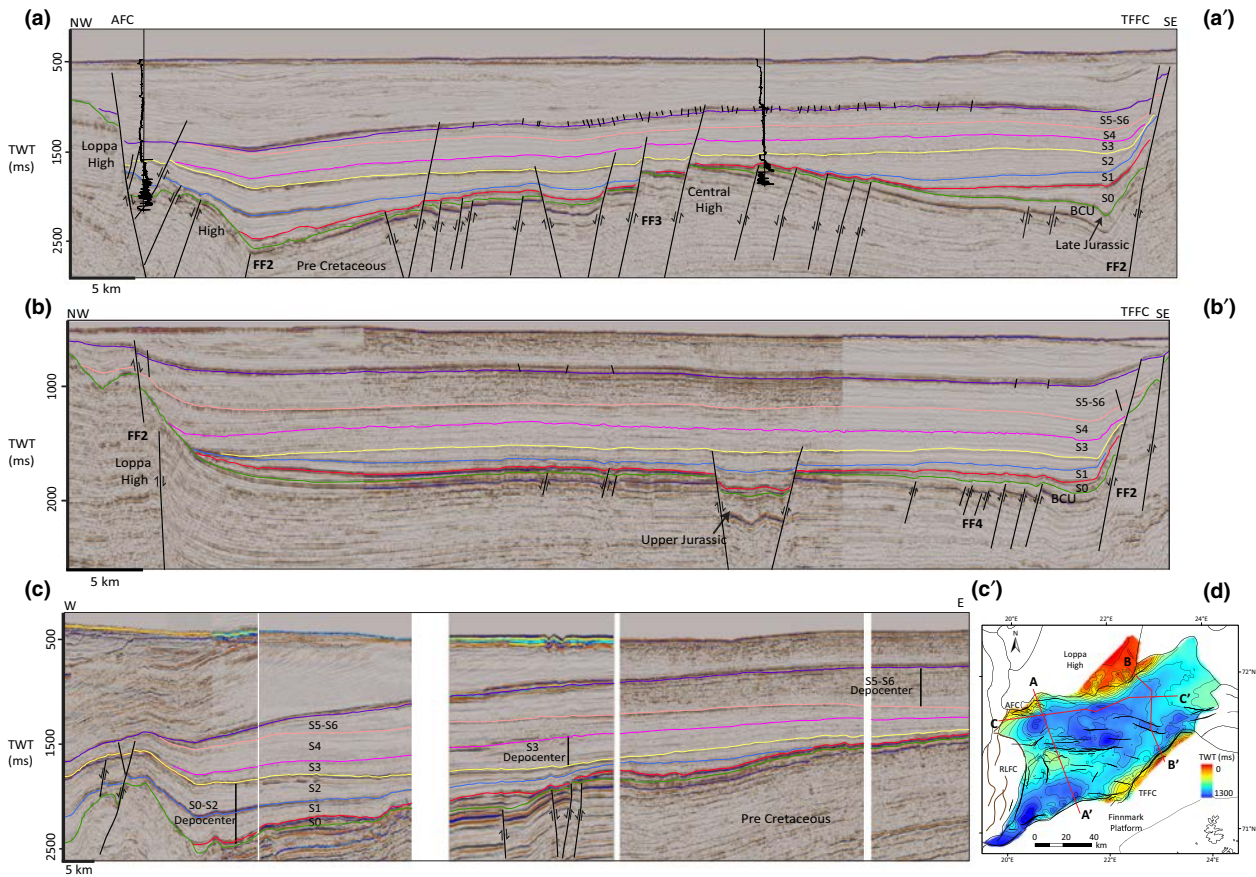


Fig. 2. Regional seismic sections showing the seven genetic sequences (S0 to S6) interpreted in this study. (a) Section located in the western part of the Hammerfest Basin. Note the location of the central high, the structural high associated with the Asterias Fault Complex (AFC) and the Troms–Finnmark Fault Complex (TFFC) to the south. (b) Section located in the eastern part of the basin. Note that the central part of the basin is less faulted and have a gentler gradient than in the west. Note that S5 and S6 were deposited in the SE part of the Loppa High. (c) Section located in the northern part of the basin. Note the migration of the depocenters to the east. (d) Lower Cretaceous time thickness map with the main active faults.

in proximity to the RLFC, suggesting an influence of the Aptian event in the Hammerfest Basin.

Stratigraphy

During the latest Volgian to earliest Valanginian, a regional unconformity (and its correlative surface) known as the Base Cretaceous Unconformity (BCU) was formed in the Barents Sea (Fig. 3b) (Århus *et al.*, 1990; Lundin & Doré, 1997; Mørk *et al.*, 1999). The Lower Cretaceous succession in the Hammerfest Basin is divided into three formations: Knurr, Kolje and Kolmule formations, which consist of claystone with minor limestone and sandstone interbeds deposited in an open-marine environment (Fig. 3) (Dalland *et al.*, 1988; Mørk *et al.*, 1999). Laterally, discontinuous sandstone beds and conglomerate packages have been identified in the Knurr and Kolmule formations forming wedges along the margins of the Hammerfest Basin (Mørk *et al.*, 1999; Seldal, 2005), suggesting a major

variability in the depositional environment. The depositional setting for these wedges is interpreted to be submarine fans in the south-western part of the study area (Seldal, 2005) and mainly offshore transition to continental for the wells 7120/1–2 and 7120/2–2 in the north-western part of the basin (Fig. 1) (Sandvik, 2014). Due to the lateral variability of the facies, uncertainties in the correlation of formations and the limited age control in the Lower Cretaceous succession, a sequence stratigraphic framework of seven genetic sequences (S0–S6) bound by flooding surfaces (*sensu* Galloway, 1989) is used in this study for well and seismic correlations (Fig. 3) (Marín *et al.*, 2017). The sequences are defined using stacking patterns in the Gamma Ray (GR) logs and lap terminations on seismic data, and their boundaries are marked by downlaps and high GR values (Fig. 3a). The sequences represent a time span of 5–10 million years and can be correlated through all the basin and in areas such as the eastern Barents Sea and partially

with Svalbard (Grundvåg *et al.*, 2017 and Marín *et al.*, 2017). They are also partially comparable with the North Atlantic cycles described by Jacquin *et al.* (1998). These sequences are interpreted as being controlled by regional factors, although locally modified by the fault activity in the Hammerfest Basin, as pointed out by Sneider *et al.* (1995) for the North Sea. The oldest sequences, 0 and 1 (S0 and S1; Boreal Berriasian/Volgian–Valanginian and Hauterivian–early Barremian), are approximate time correlative with the Knurr Formation. Sequence 2 (S2; early Aptian–middle late Aptian age) is partially time correlative with the Kolje Formation, and the youngest sequences 3–6 (S3–S6; Albian–Cenomanian) are approximate time correlative with the Kolmule Formation (Fig. 3a).

METHODS

Two- and three-dimensional, conventional reflection seismic data covering the Hammerfest Basin were provided by the Norwegian DISKOS database (Fig. 1). The seismic data quality varies and has frequencies ranging from 10 to 50 Hz. A total of 12 wells with a full suite of logs were included in this

study (Fig. 1). Detailed sedimentological log description for intervals of six available cores is presented (7120/2-2, 7120/2-1, 7120/2-3S, 7120/6-3S, 7120/1-2 and 7120/10-2).

In this study, the age control for the three oldest sequences (i.e. S0–S2) is improved (cf. Marín *et al.*, 2017). Furthermore, a biostratigraphical framework for the four youngest sequences (i.e. S3–S6) is provided here. To achieve this, dinocyst analysis on samples collected from wells 7121/5-2 (S0–S6) and 7122/2-1 (S0) was performed (Fig. 3). Samples from well 7122/2-1 were collected from a sediment core. Palynological slides from well 7121/5-2 were prepared from mainly ditch cutting and only few sidewall core samples. Palynological slides from well 7122/2-1 and the upper part of the 7121/5-2 well were prepared at the Geological Survey of Denmark and Greenland (GEUS) following methods described by Nøhr-Hansen (2012).

The age frame is tied to the seismic with synthetic seismograms (Fig. 3c). Time thickness maps and seismic facies are described for each sequence. The seismic facies description and interpretation is based on information such as: foreset angles, presence or absence of topsets and bottomsets, external geometries (e.g. mound, wedges), internal configurations (e.g.

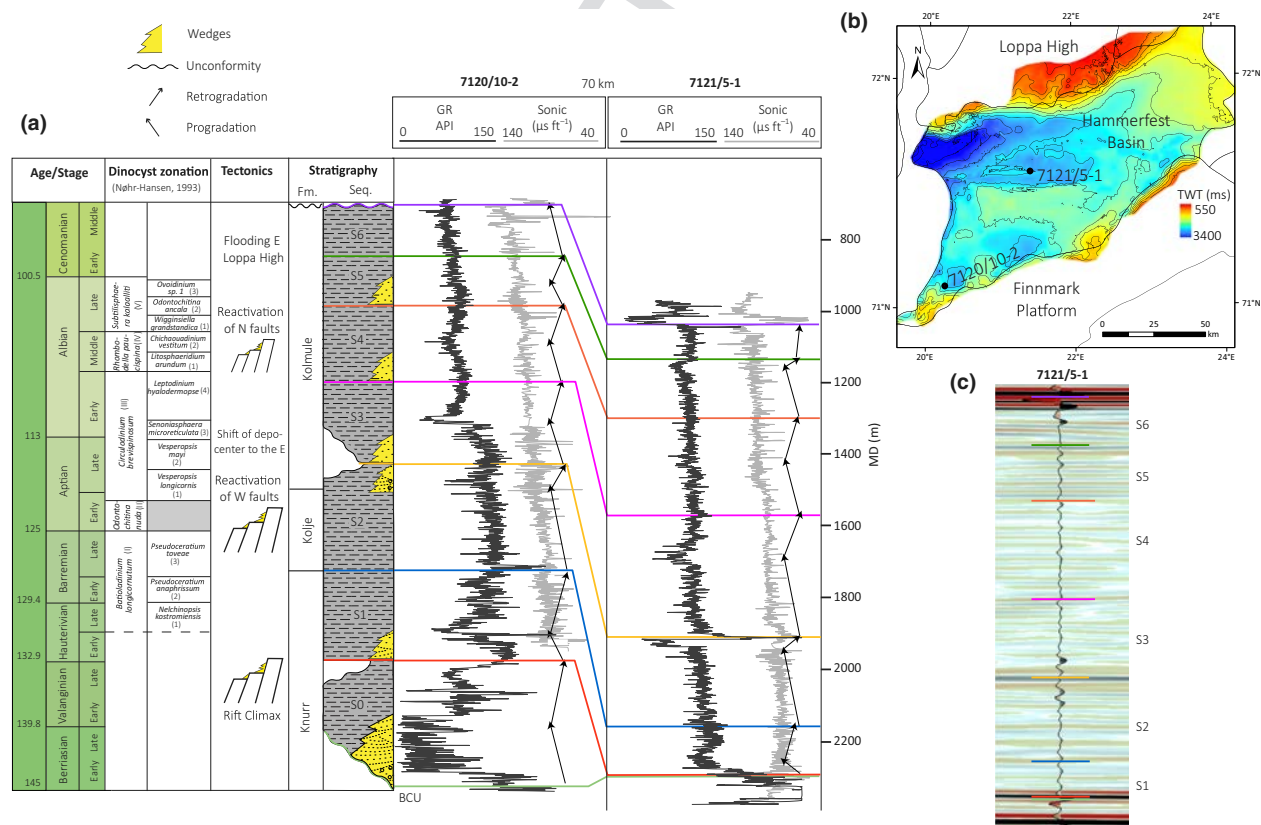


Fig. 3. (a) Well correlation showing the seven sequences and their defined stacking patterns. Formation ages from Mørk *et al.* (1999). Wedges are observed in most of the sequences in different areas of the basin; (b) structural map of the BCU; (c) synthetic seismogram for well 7121/5-1.

chaotic, continuous reflectors), amplitude and continuity of the reflectors. Some of the seismic lines with clinofolds are converted to depth and decompacted (for details, see Marín *et al.*, 2017) in order to get the original depositional approximate geometry (Deibert *et al.*, 2003; Salazar *et al.*, 2015). The sedimentological interpretation of the seismic facies is constrained by cores and GR logs.

In this study, we refer to the full fan-shaped geometry composed of different architectural elements as submarine fans, whereas lobe is referred to as the down-dip part of the submarine fan formed at the end of a channel (Normark, 1978; Walker, 1978; Stow *et al.*, 1996; Grundvåg *et al.*, 2014).

RESULTS

Age model

Dinocysts from sequence 0 (S0) were studied from the sediment core in well 7122/2-1. The basal part of S0 yields (possibly reworked) late Early to early Middle Jurassic dinocysts, such as *Nannoceratopsis gracilis*, *Susadinium* sp., *Susadinium scofoides* and *Parvocysta nasuta*. The upper part of S0 in 7122/2-1 yields *Pseudoceratium anaphrissum* which suggests an early Barremian age. The dinocyst assemblage from the base of S0 in well 7121/5-2 is similar to the assemblage from the Barents Sea described by Århus *et al.* (1990) and dated to the Boreal Berriasian/Volgian. The middle and the upper parts of S0 in 7121/5-2 are of Valanginian age. In Marín *et al.* (2017), the middle and the upper parts of S0 in the 7120/10-2 well were tentatively dated as latest Ryazanian to Valanginian or younger. In the same well, APTEC (2007) observed palynomorphs from Norian–Rhaetian, Late Callovian–Middle Oxfordian and Late Pliensbachian to Early Bajocian and interpreted them as reworked. Summarizing all observations, S0 is dated to Boreal Berriasian/Volgian–Valanginian or to early Barremian. The sequence is also characterized by a significant degree of reworking.

In contrast to the material analysed in Marín *et al.* (2017), the dinocysts from sequence 1 (S1) in the well 7121/5-2 are abundant and diverse. The most characteristic dinocysts are *Batioladinium longicornutum* and *Pseudoceratium anaphrissum*. Dinocyst assemblages narrow the age frame for the sequence and suggest that the base of S1 is of upper Hauterivian age, whereas the middle and upper part is early Barremian. In Marín *et al.* (2017), only the middle part of sequence 2 (S2) was studied for biostratigraphy and tentatively dated to middle late Aptian. Dinocyst assemblages from S2 in 7121/5-2 yield, for example, *Circulodinium brevispinosum*. This suggests that S2 is of early Aptian to

earliest Albian age. Within sequence 3 (S3), the dinocyst preservation is moderate and the diversity is rather low. The assemblages yield dinocysts with long ranges. The best age constraint is given by the single SWC sample from the middle part of the sequence, which yields *Surculosphaeridium longifurcatum*. In the Boreal realm, the first appearance of the species is dated to 111.16 Ma, (i.e. the earliest Albian; see Williams *et al.*, 2004). Sequence 4 (S4) yields, for example, *Chichaouadinium vestitum* and *Wigginsella grandstandica*. The dinocyst assemblages suggest that the lower part of the sequence is (tentatively) of middle Albian, whereas the upper part is of late Albian age. The most important dinocysts observed within sequence 5 (S5) are *Endoceratium turneri* and *Apteodinium grande*. Our results indicate latest Albian to earliest Cenomanian age for S5. Sequence 6 (S6) yields, for example *Endoceratium dettmanniae* and ‘*Sidridinium*’ sp sensu Bailey (2017). The dinocyst assemblage suggests that S6 spans early to late Cenomanian age.

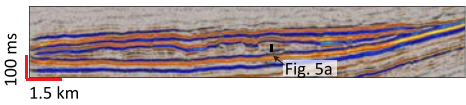

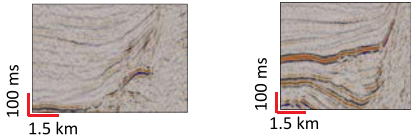
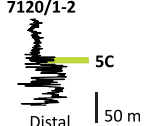
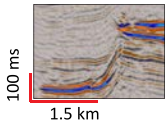
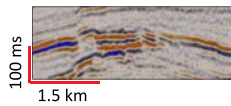
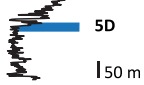
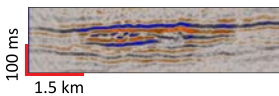

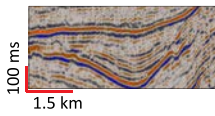
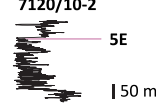
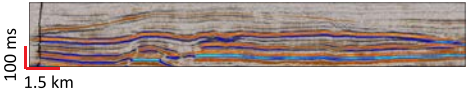
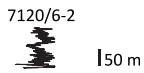

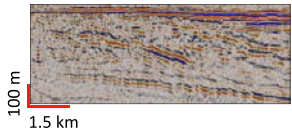
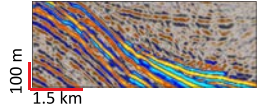
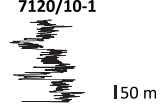
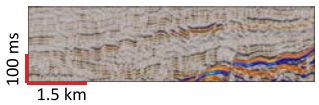
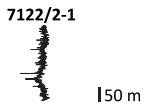
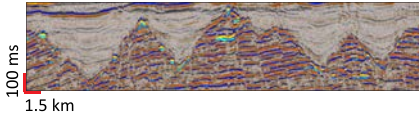
Fault Families

Four main types of fault families (i.e. faults with similar strike and age), affecting the Lower Cretaceous sequences, are observed in the study area (Figs 1 and 2). *Fault family 1 (FF1)* is constituted by normal faults with a NNE–SSW strike and is located in the western part of the basin. Most of the faults in FF1 belong to the RLFC in the boundary with the Tromsø Basin and they offset all the sequences. The throw of the RLFC has been interpreted to be more than 5000 ms TWT (Gabrielsen *et al.*, 1990). *Fault family 2 (FF2)* is constituted by NE–SW striking normal faults of the segmented TFFC in the south and to the discontinuous AFC in the north (Figs 1 and 2). The TFFC and AFC in the NW offset all the sequences and throws can be up to 1100 ms TWT (Fig. 2a). The NE faults only offset younger sequences than S3 (Fig. 2b). *Fault family 3 (FF3)* is constituted by E–W striking normal faults and is located in the central part of the basin. Some of the faults offset all the sequences and some of them stop at the BCU level. The faults can be linked or isolated (Figs 1 and 2). *Fault family 3* has throws up to 200 ms TWT. *Fault family 4 (FF4)* is constituted by NW–SE striking normal faults, and they are usually isolated. *Fault family 4* is located in the eastern part of the study area, affecting the S0–S2 or stopping at the BCU level. Throws can be up to 400 ms TWT (Figs 1 and 2b).

Seismic facies

Twelve seismic facies related to the Lower Cretaceous fault activity have been defined and are summarized in Table 1.

Table 1. Summary of the seismic facies recognized in the Lower Cretaceous succession of the Hammerfest Basin.

Facies description	Interpretation	Example	GR Pattern	
			0	150
A Mound, variable internal reflector, discontinuous, chaotic, bidirectional downlaps	Coalescent fan deltas	 Fig. 5a	7122/2-1	 5A 50 m
B1 Wedges, internal chaotic to continuous. Prograding reflectors are common	Continuous slope system/aggradational fan deltas		7120/1-2	 5C Distal 50 m
B2 Small scale wedges, high amplitude reflectors	Talus, fringes, fault degradation		Not drilled	
C1 Lens, internal high amplitude discontinuous reflectors.	Slope channel system		7120/2-3S	 5D 50 m
C2 Lens, internal high amplitude discontinuous reflectors.	Turbidite lobe fed by a point source		7120/6-3S	 5F Distal 50 m
D High amplitude continuous parallel reflectors, bidirectional onlaps	Turbidite lobe		7120/10-2	 5E 50 m
E Medium to low amplitude parallel reflectors. Mounds are common.	Lobe fringe/off axis environment		7120/6-2	 50 m
F1 Low angle clinoforms (1°), with a height of 40-100 m	Sediments prograding in a shelf		Not drilled	
F2 Clinoforms with foreset angles of 2-5° and a height of 80-210 m	Shelf-margin clinoforms		Not drilled	
F3 High angle clinoforms (2-15°), a height of 80-200 m and associated with a scarp	Progradational fan deltas/shorelines		7120/10-1	 150 m
G Chaotic, medium to low amplitude reflectors, with imbrications	Mass transport complexes		7122/2-1	 150 m
H Incisions	Incised valleys, gullies or scours		Not drilled	

COLOR

Facies A (Mounds)

Description

Mounds with variable internal reflectors can be discontinuous or chaotic. Truncations are locally observed (Table 1). Clinoforms are sometimes identified in the dip direction, with a height of 40–80 m and bidirectional downlaps in the strike direction (Fig. 4a,b). Facies A was penetrated by well 7122/2-1, and the GR log shows a blocky pattern (Table 1). A fifty-metre-long core shows sandstones with pebbles and shell debris (Fig. 5a; Table 2).

Interpretation

Mounds (facies A) are interpreted as shallow marine coalescent fan deltas (*sensu* Dabrio, 1990) (Fig. 5a; Table 1). The sedimentological characteristics of well 7122/2-1 indicate shallow marine to a possible transgressive shoreface environment (Table 2). The height of the clinoforms (40–80 m) reveals a prograding shoreline/fan (Fig. 4a). The truncations are interpreted as a local unconformity, followed by a flooding event marked by the top of S0.

Facies B (Wedges)

Description

Facies B is always observed next to a fault scarp and is subdivided in B1 and B2 (Fig. 4b,c,d; Table 1). Facies B1 is characterized by wedges with a high slope angle (approx. 5–6°) and with internal chaotic or continuous reflectors, forming a laterally continuous feature next to the main fault scarps. Topsets are usually not observed (Fig. 4a; Table 1). Small wedges (facies B2) are located in narrow areas close to fault planes (Table 1).

Interpretation

The lateral continuity of facies B1 indicates the presence of laterally continuous slope deposits alike the slope system described by Leppard & Gawthorpe (2006). These deposits are interpreted as coalescing fans consisting of gravity flow deposits. The lack of topsets in this facies suggests direct deposition to the slope, presumably detached from the source, as described by Surlyk (1989) in East Greenland. Some of these wedges were probably fed by fan deltas which typically have a narrow subaerial part with low preservation potential and a subaqueous part, which in deep-marine settings tend to aggrade due to the high amount of available accommodation space (Surlyk, 1989; Dabrio, 1990; Reading & Collinson, 1996). Facies B2 is more restricted to narrow areas close to the bounding faults, suggesting talus or fault degradation

complexes, similar to those described by Surlyk (1978 and) Surlyk (1989) and Henstra *et al.* (2016). Wells 7120/2-2 and 7120/2-1 penetrated facies B1 in the north-western part of the basin and the amount of sandstone varies (Fig. 5a,b; Table 2). Wedges (facies B1) in the north-western part of the basin are interpreted as talus cones formed in shallow water. This is supported by sedimentological observations of wells 7120/1-2 and 7120/2/2, which indicate the presence of offshore transition deposits with interbedded gravity flow deposits, grading upward into shallow marine (Fig. 5a,b; Table 2) (Sandvik, 2014).

Facies C (lens)

Description

Facies C is lens shaped, narrow in the proximal part (facies C1) and wider in the distal part (facies C2), with internal high amplitude and discontinuous reflectors (Table 1). Facies C1 and C2 were drilled in wells 7120/2-3S (proximal) and 7120/6-3S (distal), respectively. The core of well 7120/2-3S penetrated fining upward units of poorly sorted conglomerates, sandstones and siltstones (Fig. 5d,f; Table 2). The distal well 7120/6-3S found claystones and siltstones interbedded with normally graded sandstone beds (Fig. 5f; Table 2).

Interpretation

The fining upward conglomerate beds drilled in well 7120/2-3S (facies C1) are interpreted as gravity flow deposits emplaced in a slope conduit (Fig. 5d; Table 2). The normal grading sandstones and the trace fossils in well 7120/6-3S (distal part of facies C2) indicate deposition by turbidity currents in a lobe fringe setting (Fig. 5f; Table 2) (Kneller, 1995; Grundvåg *et al.*, 2014). Based on seismic facies, attribute maps and sedimentological observations, facies C1 and C2 are interpreted as a submarine fan fed by a single point source, where the discontinuous reflectors may represent channels (Fig. 7a,b; Table 1).

Facies D (continuous reflectors)

Description

Parallel reflectors with high amplitude (facies D) (Fig. 4c,d). This facies is commonly observed adjacent to facies B1, where high slope angles (approx. 5–6°) are replaced by parallel reflectors in the southern part of the basin. (Fig. 4c). Facies D was drilled by well 7120/10-2 (Fig. 5e). The GR log shows a blocky pattern, which tends to be more heterolithic towards the top. An 8.5 m core in the upper part of the unit shows a tripartite subdivision: a) a lower heterolithic unit; b) a

1 middle homogenous sandstone, thick-bedded and
 2 capped by a thin mudstone and a muddy sandstone
 3 bed; and c) an upper sandstone-dominated unit
 4 (Fig. 5e; Table 2).

6 Interpretation

7
 8 Facies D is interpreted as a turbidite lobe. This facies
 9 was penetrated by well 7120/10-2, and its lower het-
 10 erolithic part is interpreted as a distal/off axis tur-
 11 bidite lobe in a slope setting (see Grundvåg *et al.*,
 12 2014 for similar deposits). Trace fossils that can be
 13 attributed to the *Zoophycos* Ichnofacies, common in
 14 slope settings (Frey & Pemberton, 1985), support the
 15 interpretation (Figs 4d and 5e; Table 2). The fans
 16 middle part is more sandstone-dominated and was
 17 probably deposited by high-density turbidity currents
 18 in a proximal turbidite lobe. The upper unit, which is
 19 upward fining, may suggest deposition in a lobe fringe
 20 to proximal lobe environments (see Grundvåg *et al.*,
 21 2014 for similar deposits) (Table 2). The relationship
 22 between the steep wedges (facies B1), deposited next
 23 to the TFFC and the parallel reflectors with high
 24 amplitude (facies D) (Fig. 4e), presumably reflects the
 25 transition of deposition from mass movements or cohe-
 26 sive debris flows in the proximal part (facies B1) to a
 27 fully turbulent flow (facies D, supported by the obser-
 28 vations in well 7120/10-2). This is a consequence of a
 29 change in the slope gradient and an increase in water
 30 depth (Figs 4d and 5e and Table 2), as described by
 31 Lowe (1982); Mulder & Alexander (2001); Leppard
 32 & Gawthorpe (2006); Henstra *et al.* (2016) in other
 33 settings.

36 Facies E

37 Description

38 Parallel reflectors with medium-to-low amplitude (facies
 39 E). This facies can occur as mounds with internal contin-
 40 uous reflectors (Table 1). Facies E is commonly observed
 41 in the central part of the basin. The Gamma Ray log from
 42 well 7120/6-2 (Table 1) shows mainly high values with
 43 thin intervals of low values.

47 Interpretation

48 Facies E identified in the central part of the basin is inter-
 49 preted as a lobe fringe facies, where the thin intervals of
 50 low GR values suggest thin-bedded turbidite deposits
 51 (see Surlyk, 1978; Grundvåg *et al.*, 2014 for similar exam-
 52 ples). This facies can have mound shapes, which are inter-
 53 preted as the finger-like protrusion from the distal part of
 54 a lobe (Prélat *et al.*, 2009), enhanced during compaction
 55 (Shanmugam & Moiola, 1991).

Facies F (clinofoms)

Description

Facies F is subdivided into three groups: 1) facies F1 is
 characterized by clinofoms with a height of 40–100 m
 and foreset angles of 1°; 2) facies F2 is characterized by cli-
 nofoms with a height of 80–210 m and foreset angles of
 2–5°; and 3) facies F3 is characterized by clinofoms asso-
 ciated with fault planes, with a height of 80–200 m and
 foreset angles of 2–15° (Table 1). Facies F3 was pene-
 trated by well 7120/10-1, and its GR log shows intervals
 with low values (Fig. 7d).

Interpretation

The clinofoms are interpreted based on their height
 (Steel *et al.*, 2008; Helland-Hansen & Hampson, 2009;
 Sanchez *et al.*, 2012). Facies F1 is interpreted as prograd-
 ing sediments in a shelf environment; facies F2 is inter-
 preted as shelf-margin clinofoms (see Marín *et al.*, 2017
 for details); and facies F3 is interpreted as prograding fan
 deltas/shorelines due to their proximity to a scarp
 (Table 1) (i.e. Loppa High and the Finnmark Platform).

Facies G

Description

Facies G is characterized by chaotic reflectors with imbrica-
 tions. The GR log of well 7122/2-1 shows mainly high
 values with thin intervals of low values (Table 1).

Interpretation

Facies G is interpreted as mass transport complexes
 (MTCs), where the imbrications represent syndeposi-
 tional thrusts (*sensu* Moscardelli & Wood, 2008).

Facies H

Description

Facies H is characterized by incisions of different dimen-
 sions, which can have more than a couple of hundred
 metres, to below the seismic resolution (Fig. 6c; Table 1).

Interpretation

Facies H is interpreted as incised valleys, gullies or
 scours.

Lower Cretaceous sequences

The main depocenters, geometries, lateral variability and
 geographic distribution of the seismic facies are described
 below for each sequence (Figs 8 and 9).

Sequence 0 (S0)

Sequence 0 is present across the entire Hammerfest Basin, except in some small areas in the northern, central and southern parts, where it onlaps onto the Loppa High or uplifted footwalls (Figs 8a and 4e). There are isolated and segmented depocenters, located next to the main boundary faults of FF2 and north from the central high, associated with FF3 (Figs 1 and 8a). The thickness of this sequence is not constant, and its maximum value is 465 ms TWT. The main seismic facies recognized in S0 are as follows: 1) facies A (mounds) observed mainly in the N-NE part of the basin, forming a linear belt of 70 km long (Fig. 9a); 2) facies H (incisions) are closely related to facies A. Facies H are located in the southern part of the Loppa High, where they are observed until S3 and have a NW-SE to N-S direction (Figs 7a and 9a; Table 1) or together with facies A, with a NE-SW to E-W direction (Figs 9a and 4a). Additionally, facies H is also identified in the central high (Fig. 4e); 3) facies B1 (wedges) is located immediately adjacent to fault scarps and is particularly common in the boundary with the Finnmark Platform, associated with the TFFC with a length of more than 80 km (Figs 4c,d and 9a); 4) facies B2 (small wedges) are observed in association with FF3, in the central

high (Table 1); and 5) facies D (high amplitude, parallel reflectors) is commonly observed adjacent to facies B1 in the southern part of the basin (Fig. 4c,d). In the eastern part of the basin, facies D is confined to a NW-SE graben (FF4) (Fig. 9a), and 6) facies E (medium amplitude, parallel reflectors) is observed in the central part of the basin (Fig. 9a).

Sequence 1 (S1)

Sequence 1 onlaps onto structural highs in the eastern, the central and partially in the southern part of the basin (Figs 6a and 9b). Similarly to S0, the main depocenters are isolated and are located close to main boundary faults in the NW and SE, associated with FF2 and in the SW associated with FF4 (Figs 1 and 8b). The maximum thickness of S1 is 450 ms TWT. Facies E (medium amplitude, parallel reflectors) is the dominant seismic facies within S1 (Figs 4c and 6a). Facies E is located not necessarily immediately adjacent to a fault plane (Table 1). Facies B1 (wedges) is now more aerially restricted than in S0 (Fig. 9b). Two main wedge levels are identified in the north-western corner of the basin (Knutsen *et al.*, 2000; Sandvik, 2014), where the lower level belongs to S0-S1 and the second level to S2 (Figs 6b and 7b). Amplitude extraction at the top of this sequence

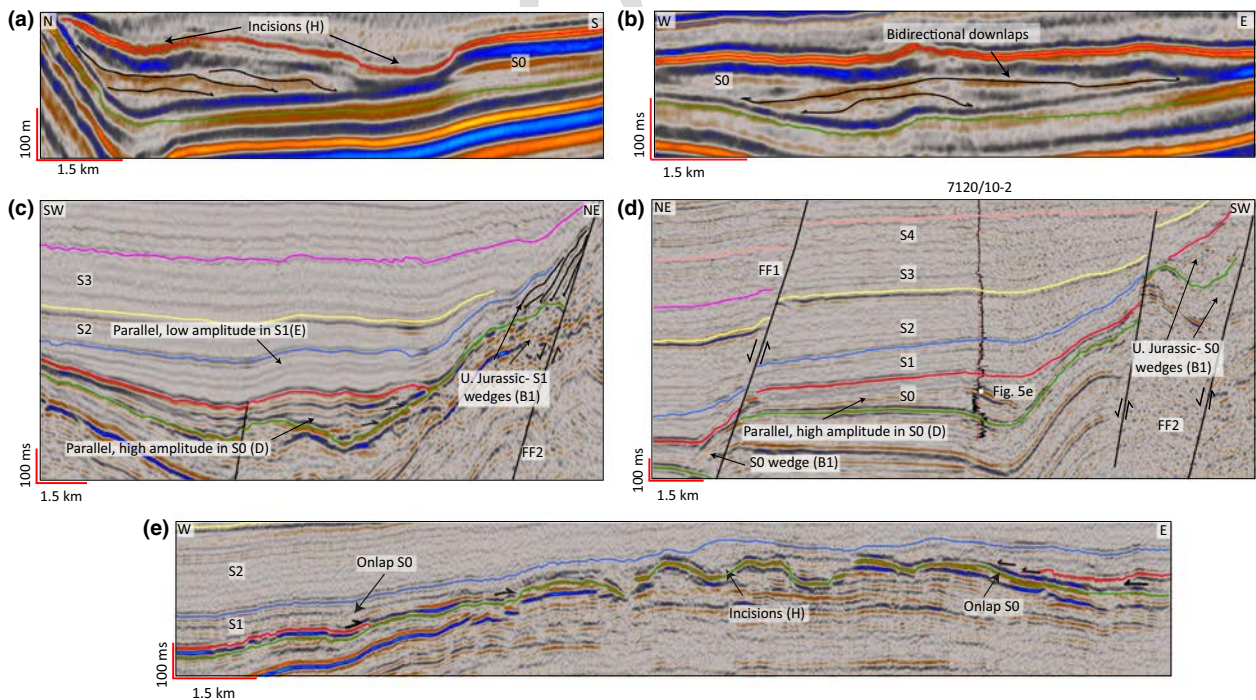


Fig. 4. Seismic lines showing the seismic facies in sequence 0 (SF of S0). (a) Prograding reflectors with associated incisions (SF H). (b) Mound with bidirectional downlaps (SF A). (c) High amplitude, parallel reflectors in S0 (SF D). Wedges (SF B1) are present next to the fault in the pre-BCU strata and in S1. (d) Wedge and spillover lobe (D). (e) Top of S0 onlaps onto the central high. Incisions (SF H) are present. Location of the seismic lines is indicated in Fig. 5a.

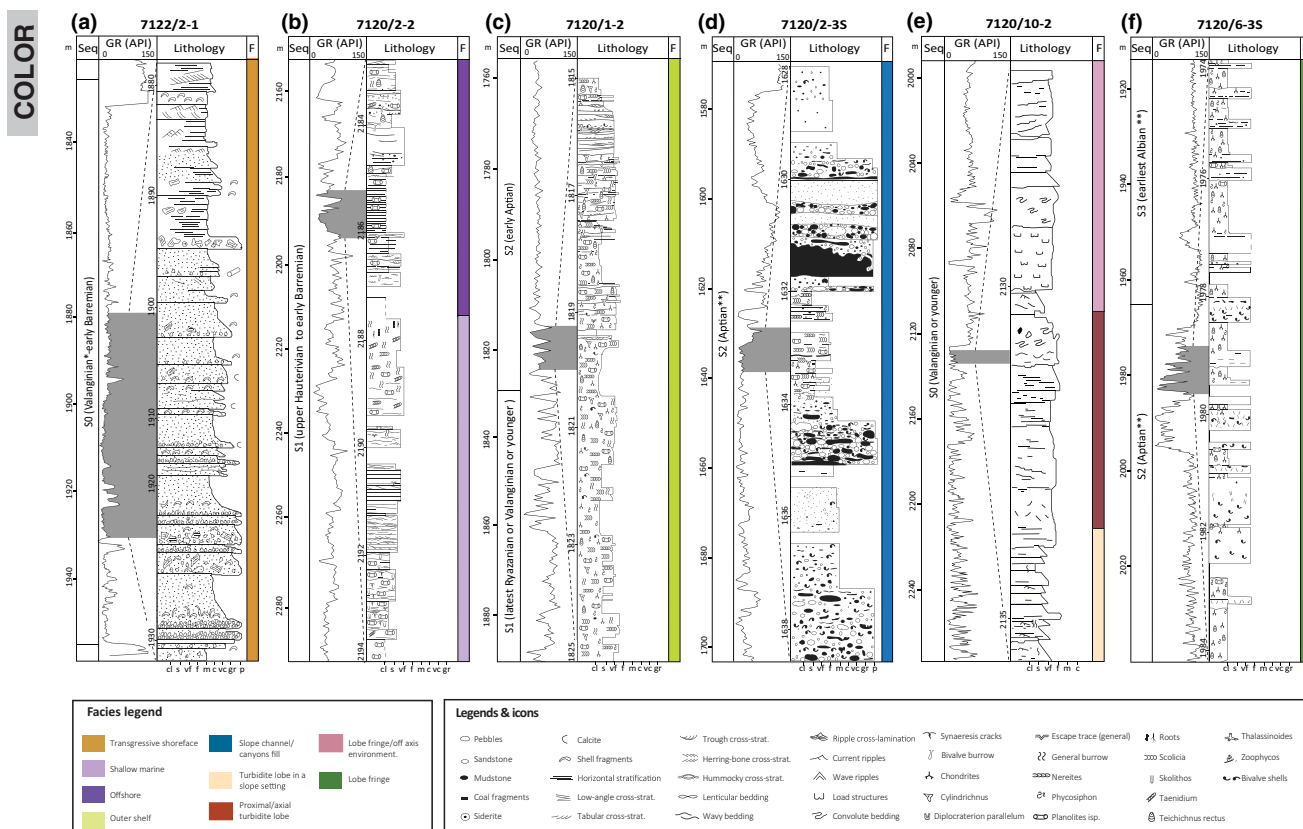


Fig. 5. Sedimentological logs of six key wells. (a) well 7122/2-1; (b) 7120/2-2; (c) 7120/1-2; (d) 7120/2-3S; (e) 7120/10-2; and (f) 7120/6-3S. Areas with missing core data are sampled for seal peels. Logs for wells 7120/2-2, 7120/1-2, 7120/2-3S and 7120/6-3S were provided by Ichron Ltd. Sedimentological log for well 7122/2-1 was provided by Harald Brunstad (Lundin Norway AS). Location of the wells is indicated in Fig. 1. *Ages from NPD (2017). **Ages are based on regional seismic correlation.

(contiguously to the south of the wedge) reveals linear patterns that are below seismic resolution. These patterns are included as part of facies H (incisions) (Figs. 6b and 6c).

Sequence 2 (S2)





Sequence 2 is present across the entire basin except on a small high in the southern and in the north-eastern part of the basin, where it onlaps against structural highs (Fig. 9c). The main depocenters are located in the north-western and south-western part of the basin associated with FF2 and FF3. A minor depocenter is located in the south-eastern part of the basin, associated with FF4 (Fig. 8c). The maximum thickness of S2 is 550 ms TWT. In S2 and younger sequences, wedges are mainly restricted to the northern and southern fault boundaries (FF2). The top of this sequence partially onlaps onto S0–S1 wedges close to the TFFC in the eastern and central parts (Fig. 4c). However, this relationship is not observed in the western segment of the TFFC. Instead, clinofolds (facies F3) prograding to the NW are observed (Fig. 7d). An amplitude extraction at 50 msec below the top of this

sequence, in the north-western part of the study area, shows two fan shapes with NW–SE direction, turning to E–W and SW–NE in the distal part (Fig. 7a). In cross section, the fan is narrow in the proximal part (facies C1) and wider in the distal part (facies C2), (Fig. 5; Table 2). Facies B1 (wedges) and facies F3 (clinofolds) are also observed in the north-western part of the basin (Fig. 7b). In addition, facies H (incisions) are present within S2, but they are not present in the south-western part of the Loppa High (Fig. 7a). Along the strike, to the E, facies B2 (small-scale wedges) is observed, which is also common in S1 and S3 next to the SE part of the Loppa High (Fig. 7a,c). A local unconformity is observed at the top of this sequence in the western part of the basin (Fig. 2c).

Sequence 3 (S3)


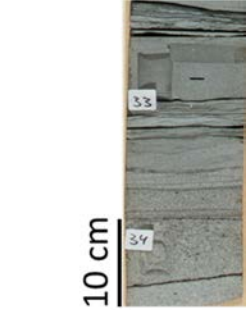
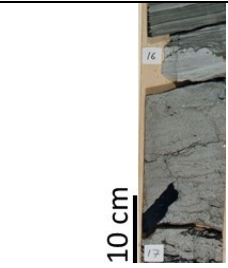
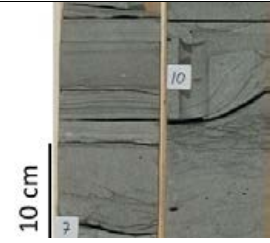
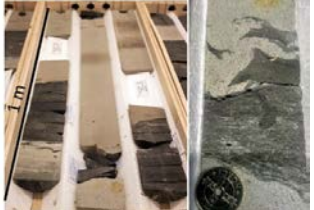
Sequence 3 is present across the entire basin, except in the north-western area where it onlaps onto S2 (Fig. 6b). The main depocenter is located in the NE. The central high affects neither this sequence nor the younger ones (Fig. 8d). The maximum thickness of S3 is 280 ms TWT. Sequence 3 is characterized by medium amplitude

Table 2. Summary of the seismic facies recognized in the Lower Cretaceous succession of the Hammerfest Basin.

	Facies example	Description	Interpretation
Fig. 5a		<p>Medium- to coarse-grained cross-stratified and plane parallel stratified sandstones. Massive beds occur locally. Occasional thin siltstone are interbedded with the sandstones. Pebbles of various lithologies and shell debris are typically occurring throughout the section. Bioturbation is very sparse and includes <i>Thalassinoides</i> and <i>Skolithos</i>. Escape traces are observed.</p>	<p>Shallow marine, possible transgressive shoreface environments.</p>
Fig. 5B		<p>Upwards thickening and coarsening grain size trends which end in cross-stratified and plane parallel stratified sandstones. Above, a heterolithic interval of mudstones and cm/dm scale of very fine- to fine-grained sandstones with current ripple cross-lamination. <i>Taenidium</i> and <i>Planolites</i> are observed. Pyrite and siderite nodules and synaeresis cracks are present.</p>	<p>Shallowing upward shoreface parasequence packages.</p>
Fig. 5B		<p>Layers of siltstones alternating with finger-thick, wave and current ripple cross laminated, silty sandstones. Soft sediment deformation and dewatering structures are found. <i>Planolites</i>, <i>Teichnicus</i>, <i>bivale burrows</i> and <i>Taenidium</i> are observed.</p>	<p>The <i>Teichnicus</i>, <i>Planolites</i> and <i>bivale burrows</i> Ichnofacies suggest Offshore conditions.</p>
Fig. 5C		<p>Heterolithic, bioturbated silty mudstones interbedded with thin, sharp-based sandstone beds either intensely bioturbated or containing swaley or wave ripple cross-lamination. Sandstones are fine to medium grained and moderately sorted. Bioturbation typically occur in transitions between the sandstone and the fine grained units. Siderite nodules are common throughout. Shell beds and shell fragments are present. <i>Teichichnus</i>, <i>Phycosiphon</i> and <i>Cylindrichnus</i> trace fossils are common.</p>	<p>The fine grained character and the <i>Cruziana</i> Ichnofacies suggests deposition in a well oxygenated open-marine shelf environment. The normally graded, sharp based sandstones with swaley or wave ripple cross-lamination indicate episodic storm deposition.</p>

(continued)

Table 2. (Continued)

Fig. 5D		<p>Decimeter- to meter-scale fining upwards units of poorly sorted clast and matrix-supported conglomerates and moderately to well sorted fine- to medium-grained sandstones and siltstones. The clasts are rounded and consist of a wide variety of multicolored carbonates, siliciclastic fragments and bivalves. In their upper part the sandstones are interbedded with claystone which thickness and abundance increase upwards. <i>Chondrites</i>, <i>Phycosiphon</i> and <i>Zoophycus</i> are observed.</p>	<p>The thick fining upward conglomerate units is interpreted as gravity flow deposits emplaced by debris flows and high density turbidity currents. The <i>Zoophycos</i> Ichnofacies and the attribute maps (Fig. 9a) indicate deposition within a slope channel/canyon environment.</p>
Fig. 5E		<p>A coarsening upwards, heterolithic unit of cm- to dm-scale, normally graded sandstone beds. The basal part contain medium-grained sandstones with mudstone clasts passing upwards into plane parallel laminated medium-grained sandstones and fine-grained current ripple cross-laminated sandstones. The beds gradually passes up into or are capped by mudstones. <i>Chondrites</i>, <i>Zoophycus</i>, <i>Asterosoma</i> trace fossils are observed.</p>	<p>The normally graded beds indicate deposition by surge-type, low-density turbidity currents. The heterolithic character indicates a distal/off axis lobe environment. The <i>Zoophycos</i> Ichnofacies is typical for continental slope, supporting the interpretation of a turbidite lobe in a slope setting.</p>
Fig. 5E		<p>A 3-4 m thick sandstone unit consisting of thick-bedded and amalgamated sandstone beds. Convolute bedding and dish structures are present. Generally, the beds are normally graded and contain rip-up mudstone clasts. The thickest beds have sharp and erosive bases. Coal fragments are common</p>	<p>Thick, normally graded sandstones rich in soft sediment deformation structures indicate deposition by high-density turbidity currents. Based on the amalgamated character of the unit, a proximal/axial turbidite lobe environment is suggested.</p>
Fig. 5E		<p>This association has a lower heterolithic part followed by thicker and amalgamated and normally graded sandstone beds dominated by dish structures and convolute bedding. The association shows an overall coarsening upward.</p>	<p>The lower heterolithic part indicate deposition in a lobe fringe/off axis environment. The amalgamated unit represent deposition in more proximal /axial lobe environments. The upward coarsening indicate that the lobe was prograding.</p>
Fig. 5F		<p>Dark grey claystones and siltstones interbedded with grey, well sorted, cm- to m-scale beds of fine- to medium-grained sandstones. The sandstone beds are normally graded and structureless. Small fluid escape traces and current ripple cross-lamination occur locally. Mudstone rip-up clasts and shell fragments are common at the base of the sandstones. <i>Chondrites</i>, <i>Teichichnus</i>, and <i>Phycosiphon</i> are present.</p>	<p>Submarine fan fringe. The normal grading of the sandstones suggests deposition by turbidity currents. The trace fossil assemblage and the amount of interbedded fines indicate a lobe fringe setting.</p>

COLOR

reflectors, highly faulted, with a polygonal pattern in map view (Fig. 10b,c). Facies G (chaotic reflectors with imbrications) are also common, (Table 1). Facies F3 (clinoforms) with a height of 80–100 m prograded across a narrow area, from the Loppa High to the SE. Furthermore, facies B1 (wedges) are present in the boundary with the Finnmark Platform in the south-eastern part of the basin (Fig. 10a; Table 1).

Sequence 4 (S4)

Sequence 4 is present across the entire basin, and the main depocenter is located in the N-NE (Fig. 8e). The maximum thickness of S4 is 310 ms TWT. Facies B1 (wedges) associated with the development of FF2 dominates this sequence in the northern part of the basin (Figs 6b, 9e and 11a). Two different types of clinoforms are observed: 1) clinoforms with a height of 100–200 m, foreset angles of approx. 4° and associated with a fault plane (facies F3); and 2) facies F1 (clinoforms), which prograded to the SW in the north-eastern part of the basin (Fig. 11b). In other areas of the basin, the reflectors are parallel with medium amplitude.

Sequence 5-6 (S5-S6)

Sequences 5 and 6 are present across the entire basin and on the south-western part of the Loppa High (Fig. 9f). The sequences are truncated by an unconformity (the top of S6) to the W (Fig. 2a). The main depocenter is located in the eastern part of the basin (Fig. 8f). The maximum thickness to S5–S6 is 560 ms TWT. Facies F2 (clinoforms with a height of 80–210 m) is observed in the north-western part of the study area, prograding to the E-SE (Fig. 6a). In other areas of the basin, the reflectors are parallel with low-medium amplitude.

DISCUSSION

Palaeogeographic evolution

Boreal Berriasian/Volgian to Barremian (S0–S1)

During the deposition of S0 and S1, there were two main sources of coarse-grained sediments in the basin: the Loppa High and the Finnmark Platform (Fig. 12a,b). The topography in the north and south was periodically renewed due to the successive uplift of the Loppa High (which started in the Late Jurassic; Wood *et al.*, 1989; Gabrielsen *et al.*, 1990 or earliest Cretaceous; Glørstad-clark, 2011) and the Finnmark Platform. Following each uplift event, the drainage was readjusted (similar to what Henstra *et al.*, 2016 described from East Greenland), forming multiple incised valleys in the south-eastern Loppa High (facies H, Figs 7a and 12a) and depositing

multiple wedge levels (Figs 6b and 7b). Reworked palynomorphs of Late Triassic to Middle Jurassic in the Valanginian sandstones are common in the downflank of the Troms-Finnmark Platform and the Loppa High (wells 7120/10-2 and 7122/2-1). The medium- to coarse-grained and well-sorted sandstones from the cores in wells 7120/10-2, 7122/2-1 and 7120/2-2 (Fig. 5a,b,e) contrast with the fine-grained Lower to Middle Triassic sandstones (Mørk *et al.*, 1999). These observations suggest that the sandstones of the Norian–Bajocian Realgrunnen Subgroup and probably the Snadd Formation (Mørk *et al.*, 1999) were at one stage deposited on the shoulders of the Hammerfest Basin (Loppa High and Finnmark Platform) and later acted as a sediment source when it became exposed during uplift. Incised valleys were partially entrenched into the Realgrunnen Subgroup, providing coarse-grained sediments during deposition of S0 and fed the shallow coalescent fan deltas, as seen in well 7122/2-1 (Figs 5a, 7a and 12a). Channels within the fans have a NE–SW to E–W direction, which contrasts with the NW–SE to N–S direction of the valleys in the Loppa High (Figs 6a and 12a). This indicates that fans were deflected to the west due to the FF3 movement (Fig. 12a). The presence of laterally continuous slope deposits along the southern margin of the Hammerfest Basin indicates that the Finnmark Platform provided sediments during the deposition of S0. The abundant reworked Mesozoic material and the very well-sorted sandstones in well 7120/10-2 suggests reworked sediments on a shoreline probably at a margin of a low-relief hinterland on the Finnmark Platform and its later redeposition as fans in the Hammerfest Basin (Fig. 12a).

The AFC in the north-western corner of the basin shows evidence of normal displacement. As a result, a first stratigraphic level containing shallow marine clastic wedges was formed (facies B1; Figs 6b and 7b). The high associated with the AFC controlled the shelf-edge location until the deposition of S2 (Fig. 12a–c). The linear features observed in the high associated with the AFC are interpreted as gullies formed in the slope (Fig. 8b,e), triggered by the tectonic activity during the early Barremian (Indrevær *et al.*, 2016). The water depth is interpreted as shallow in the northern part of the basin, based on observations from wells 7122/2-1, 7120/1-2 and 7120/2-2 and the height of the clinoforms (40–80 m) (Figs 4a and 5a,b,c; Table 2). The south-western part is interpreted to be deeper compared to the north-eastern part, supported by the succession of turbidites and *Zoophycos*-type trace fossil assemblage occurring in well 7120/10-2 (Fig. 5e; Table 2). In the central high and eastern part of the basin, the onlap relationship of S0 and S1 suggests that these two areas experienced periods of subaerial exposure (Figs 4e and 6a). Although the basin configuration is similar during S0 and S1, the observed wedges are fewer in S1 in the south-western part of the area, indicating a

COLOR

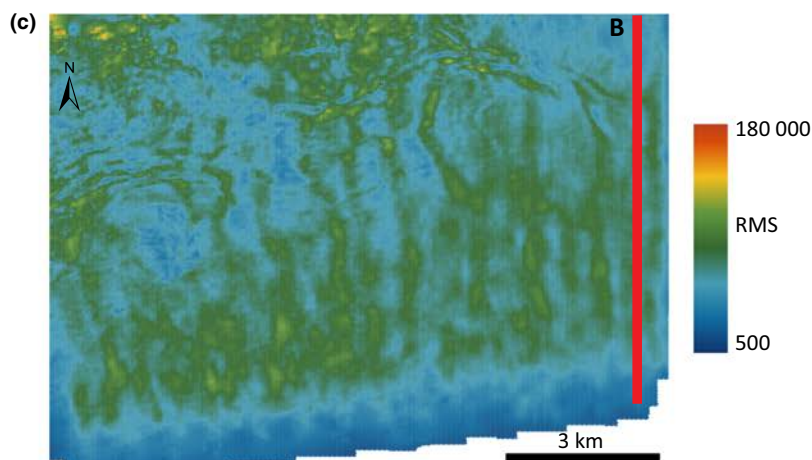
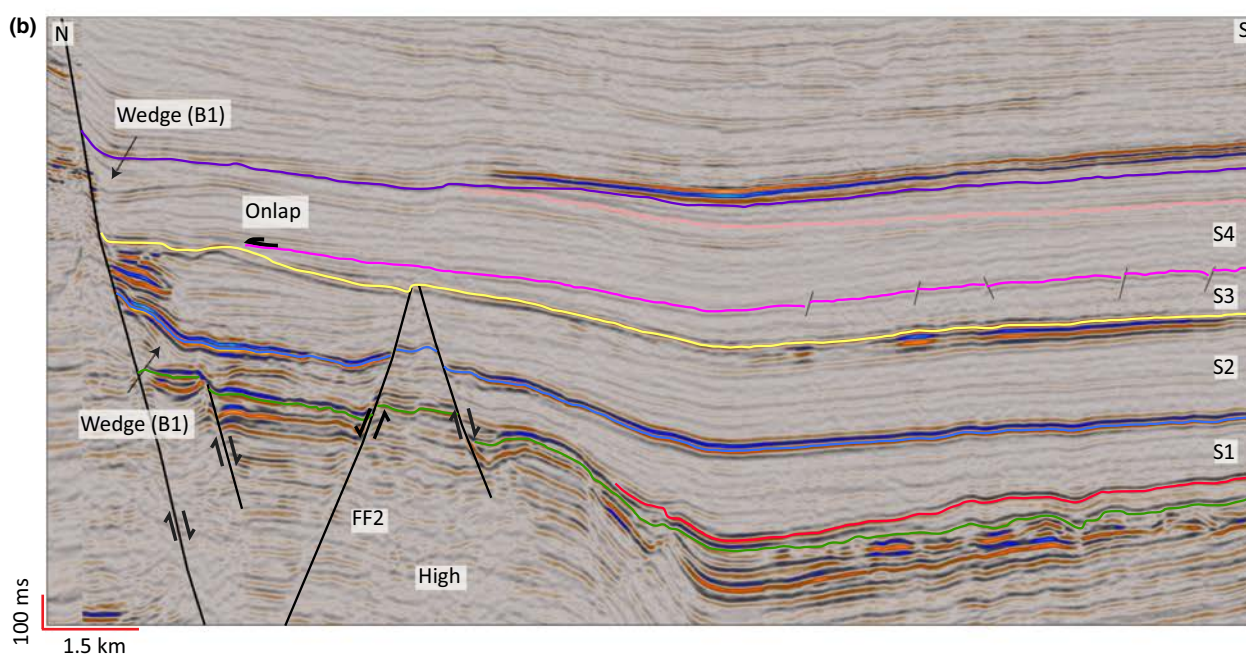
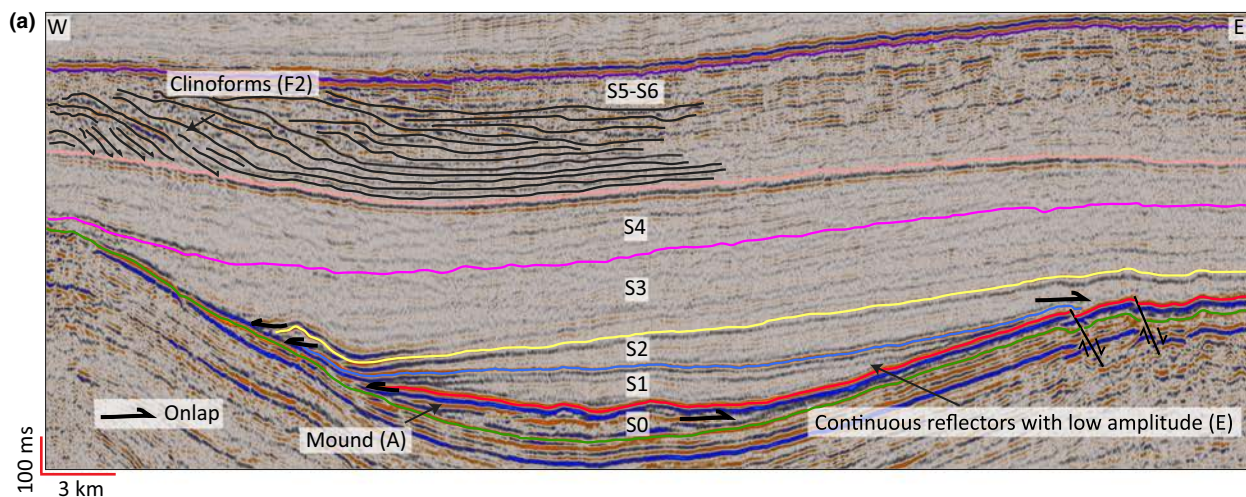


Fig. 6. Seismic lines showing the seismic facies in sequence 1 (SF of S1). (a) Sequence 1 overlies the Loppa High and the eastern part of the basin. (b) Wedge (SF B1) associated with the Asterias Fault Complex. (c) Linear features identified in amplitude extraction at the top of S1. Location of the seismic lines is indicated in Fig. 5.

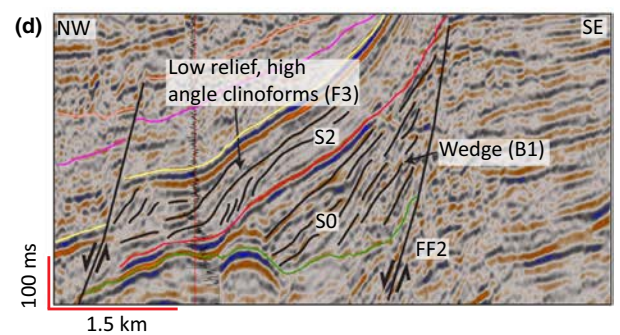
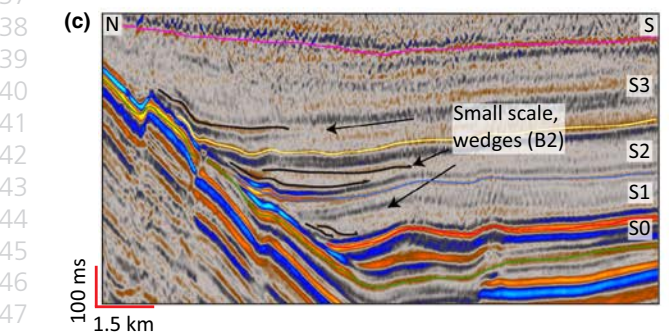
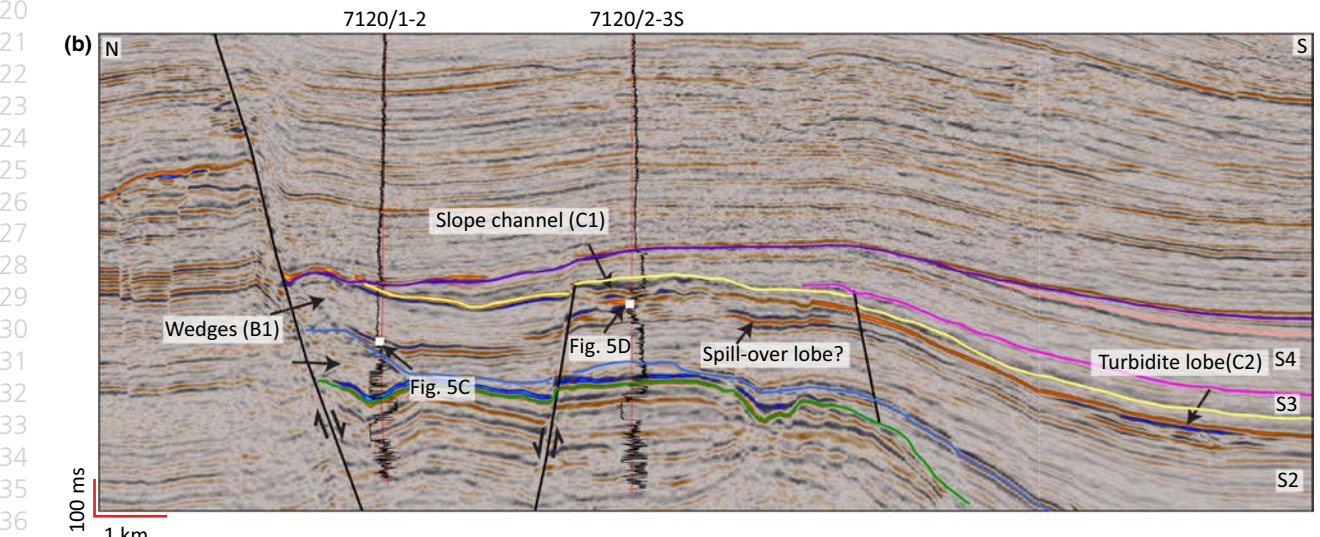
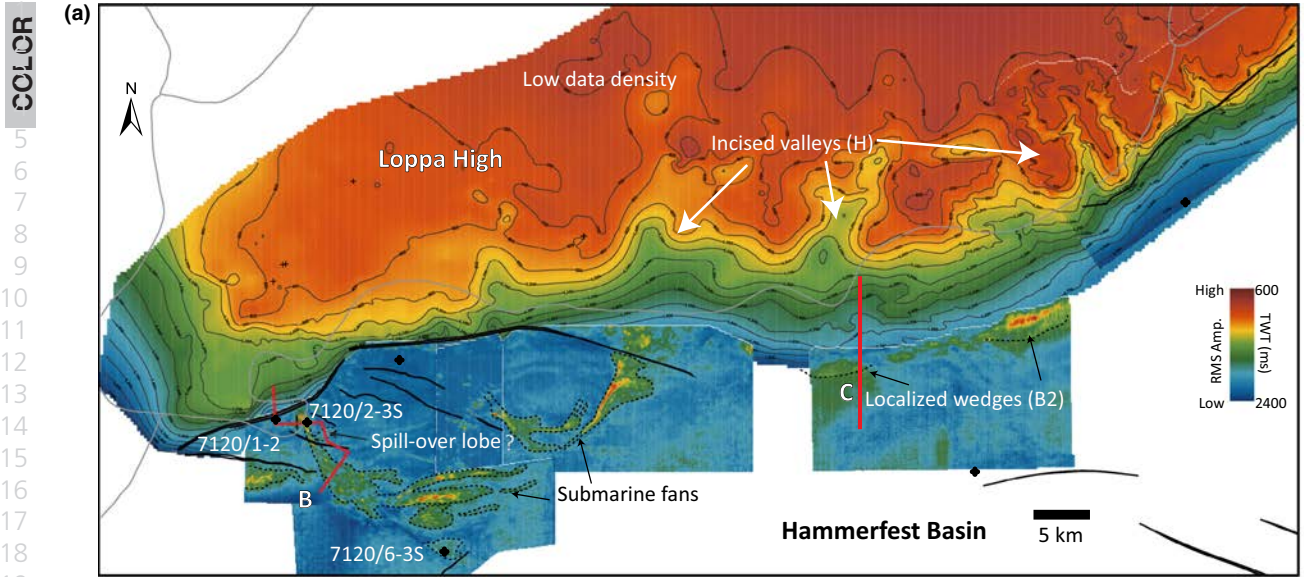


Fig. 7. Seismic lines showing the seismic facies in sequence 2 (SF of S2). (a) RMS amplitude extraction at 50 msec below the top of S2. Submarine fans are deflected to the east in the north-western part of the basin. Only localized wedges are observed in the north-eastern part. Canyons in the Loppa High are interpreted to be formed on S0. (b) Seismic line crossing the proximal and distal part of the submarine fan. (c) Small-scale localized wedges (SF B2) in S1–S3. (d) Low-relief, high-angle clinoforms (SF F3) associated with a fault scarp in the SW part of the basin.

quiescence period for the western part of the TFFC during S1.

Early Aptian to early Albian (S2)

During the deposition of S2, small wedges (facies B2) in the north-eastern part of the basin reflect that only occasional flows provided coarse-grained sediments through valleys located in the south-eastern part of the Loppa High (Figs 7a,c and 12c). This indicates a depleted source in the eastern part of the Loppa High, explained by a period of erosion reducing the topography, as suggested by Henstra *et al.* (2016) for East Greenland. In contrast, the input of sediments in the north-western corner of the basin remains important in this sequence. A second wedge level with internal prograding reflectors is associated with a fault scarp (facies F3) and is interpreted as a prograding shoreline/fan delta. The water depth in the north-western corner reached values of 140 m (based on decompacted clinofolds), but it becomes deeper towards the south, where submarine fans fed by a point source were deposited (Fig. 7a). The same relationship is observed in the southern part of the basin, where the input of

sediment is higher in the west, compared to the eastern part of the basin (Figs 7d and 12c). We suggest that the increase in the sediment supply in the western part of the basin is a combination of fault activity along the western part of the AFC and TFFC (Fig. 7a–d), and fault activity along the RLFC associated with an extensional episode that affected the Tromsø Basin within S2 (Aptian) (Faleide *et al.*, 1993). This resulted in renewed topography in the western part of the Loppa High and the Finnmark Platform (Fig. 12c), leading to an increase in the rates of erosion.

The higher erosion rate in the western part of the Loppa High could explain the lack of connected conduits for the submarine fans identified in the north-western part of the area. The flows that deposited facies C (submarine fans) were commonly deflected to the east and confined by the palaeo-topography of the basin (Figs 7a and 12c). We attribute the deflection of the submarine fans to the fault activity of the RLFC, AFC and other faults belonging to FF2. This fault activity locally tilted the north-western part of the basin and made the western-most part of the Hammerfest Basin shallow (Figs 1 and 7a).

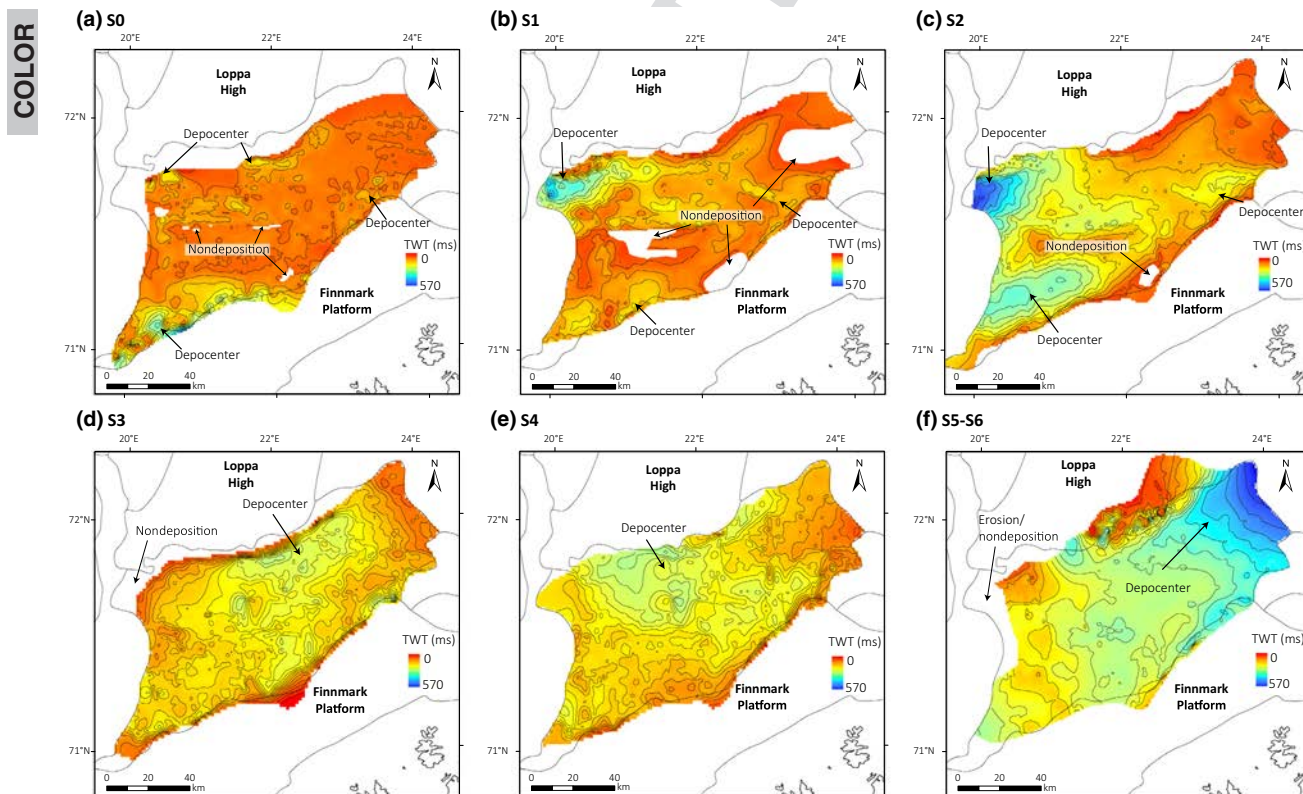


Fig. 8. Present-day time thickness maps for the sequences interpreted in this study: (a) Sequence 0 (Boreal Berriasian/Volgian to Valanginian or younger); (b) Sequence 1 (Hauterivian to early Barremian); (c) Sequence 2 (early Aptian to middle late Aptian); (d) Sequence 3 (late Aptian to earliest Albian); (e) Sequence 4 (middle Albian to late Albian); (f) Sequences 5 and 6 (latest Albian to early to late Cenomanian). Note the shift of the depocenters from the western part in S0–S2 to the central and north-eastern part of the Hammerfest Basin in S3–S6. White areas represent areas of erosion (truncation) or nondeposition (onlaps).

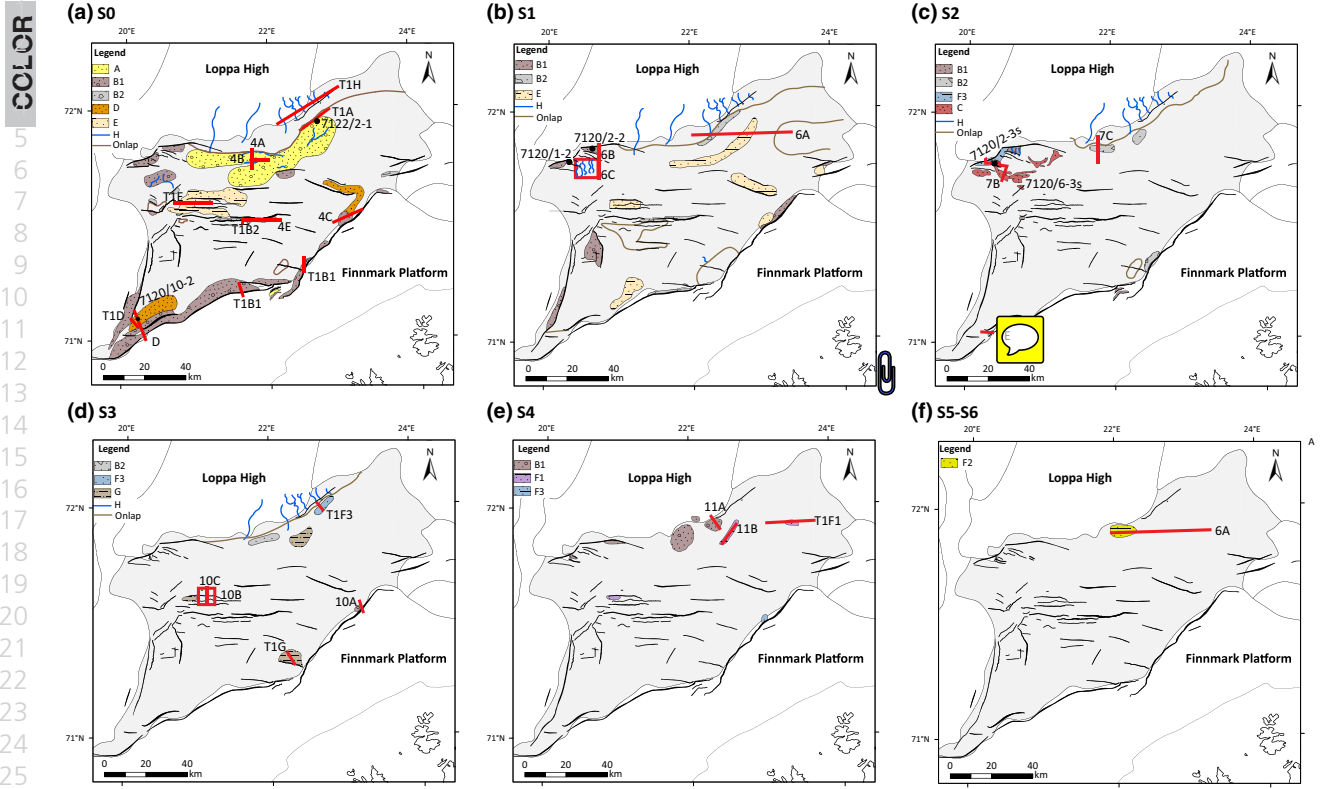


Fig. 9. Seismic facies distribution maps (a) Sequence 0 (Boreal Berriasian/Volgian to Valanginian or younger); (b) Sequence 1 (Hauterivian to early Barremian); (c) Sequence 2 (early Aptian to middle late Aptian); (d) Sequence 3 (late Aptian to earliest Albian); (e) Sequence 4 (middle Albian to late Albian); (f) Sequences 5 and 6 (latest Albian to early to late Cenomanian). The grey background colour represents parallel reflectors with medium amplitude (muddy fill with minor sand stringers). The location of the seismic facies of Table 1 is indicated as T1A–T1H.

Albian (S3–S4)

The remnant topography associated with the Finnmark Platform resulted in fan delta/shoreline progradation in the south-eastern margin (Figs 10a and 12d; Table 1). Low-angle clinoforms with a height of 40–100 m (Table 1) reflect sediments prograding in a shelf towards the SW, in the eastern part of the study area (Fig. 11b). The MTCs were probably triggered by oversteepening due to sediment loading in proximity of the shelf-edge (Table 1) (Moscardelli & Wood, 2008). Alternatively, they could be a response of the tilting of the Hammerfest Basin suggested by the shift of the depocenters from the western part in S0–S2 to the central and north-eastern part in S3–S6. This shift of the depocenters is interpreted as a consequence of the activity of the RLFC, during an extensional episode in the Tromsø Basin (Faleide *et al.*, 1993) forming the unconformity at the top of S2 (Figs 1, 2c and 4). As a result of the tilting of the Hammerfest Basin, shallower conditions are interpreted in the north-western part of the basin, supported by onlap relationships. Deeper conditions are suggested in the eastern part of the basin, supported by the height of the clinoforms (up to 200 m) (Fig. 6b). Sequence 3 is affected by

polygonal faults, suggesting fine-grained lithology (Cartwright, 2011).

Latest Albian to Cenomanian S5–S6

Climoforms that prograded from the Loppa High towards the SE (facies F2) suggest a change from an erosive to a prograding margin (Fig. 6a). Simultaneously, the south-eastern Loppa High became flooded, including the valleys located in the south-eastern part due to high eustatic sea level during the Albian to Cenomanian transition (Haq, 2014) (Figs 2b and 11a). The western part of the Loppa High remained subaerially exposed, providing sediments to allow the margin to prograde as a result of renewed uplift-induced topography (Fig. 12f).

Variables controlling the depositional systems and basin fill

Controls during rift climax

Variability along the strike of the main bounding faults: In this study, we consider the variability in the throw and the steps in the main bounding faults to be a factor

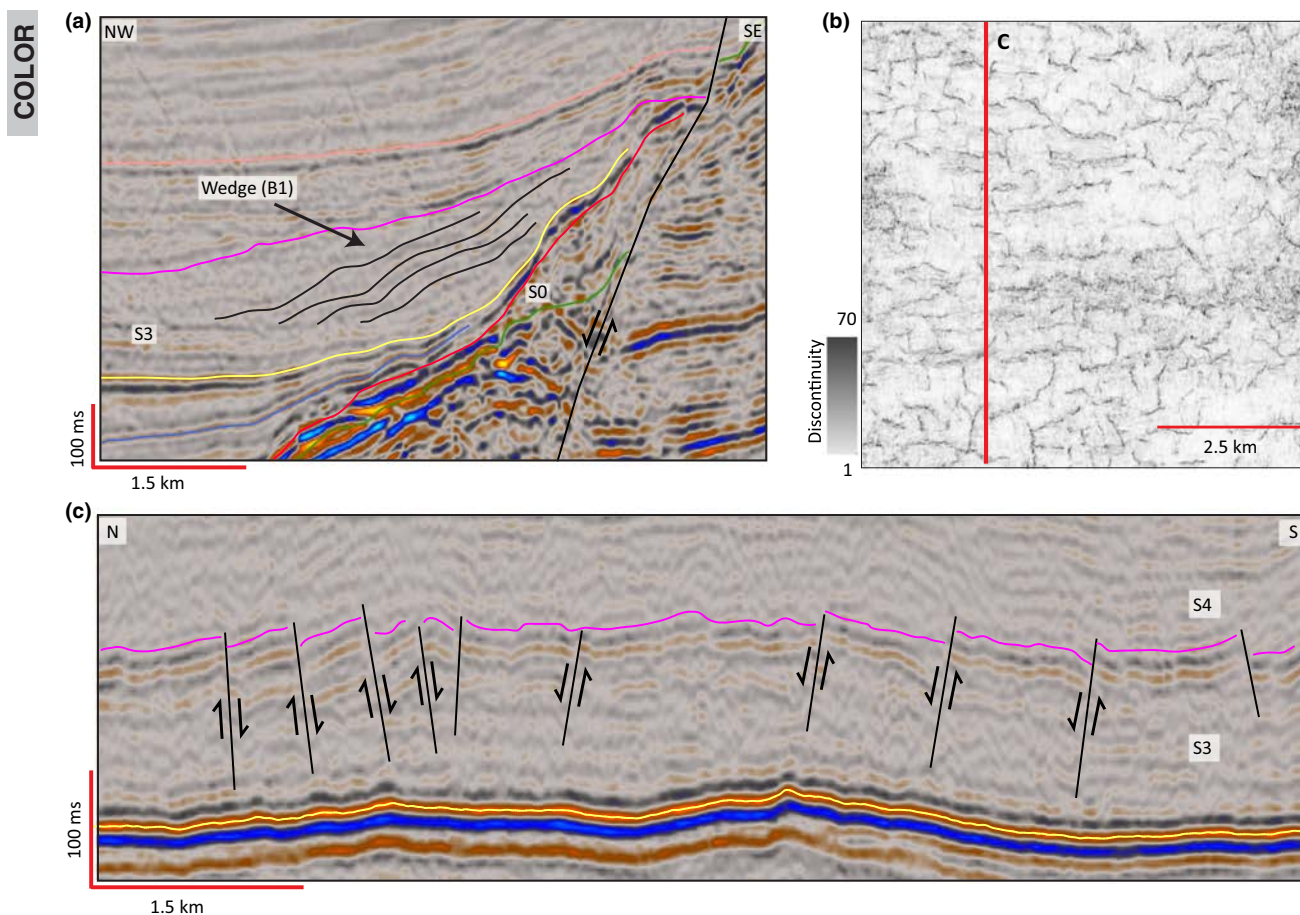


Fig. 10. Seismic lines showing the seismic facies in sequence 3 (SF of S3). (a) Wedges (B1) associated with the Troms-Finnmark Fault Complex. (b) Mean curvature attribute, showing polygonal faults. (c) Polygonal faults in cross section. Location of the seismic lines is indicated in Fig. 5.

affecting the depositional systems and the input of sediments into the basin, as it has been considered previously (Gawthorpe *et al.*, 1990; Gupta *et al.*, 1998; McLeod *et al.*, 2002; Elliott *et al.*, 2012, 2017). High accommodation space was generated in faults with higher throw, for example in the southern bounding fault (TFFC). This led to an increase in the water depth and to deposition of axial turbidite lobes in the immediate hangingwall (facies D) (Figs 9a and 12a). The accommodation space generated during the rift climax was higher in the south-western part compared to the north-eastern part, which did not have any evident fault displacement until the Albian (S4) (Fig. 11a). Lower accommodation space in the northern Hammerfest Basin led to the deposition of shallower facies (Fig. 5a). The input of sediments was affected by fault steps, for instance in the TFFC, which has been described as *en echelon* fault system (Gabrielsen *et al.*, 1990; Ahmed, 2012). In the middle part of the TFFC, a step in this fault system is suggested as a potential sediment supply entry point during the rift climax (Fig. 9).

Diachronous movement of the faults

The diachroneity of fault movement is an important control on the timing and spatial distribution of depositional systems in rift basins. In the study area, fault activity, and therefore also fault-controlled deposition and accommodation, was diachronous (Fig. 12). The BCU has been interpreted as the syn-rift to post-rift boundary in other areas of the Norwegian continental shelf (Gabrielsen *et al.*, 2001). In the Hammerfest Basin, some of the faults of FF3 and FF4 offset the pre-Cretaceous rocks, but the upper fault tips terminate below the BCU (Fig. 2). However, the BCU is commonly offset by faults of FF2 and FF1 and growth wedges are observed in the overlying sequences, indicating that the faulting in the Hammerfest Basin was initially concentrated in the central part of the basin and then in the main basin margin faults (Fig. 2). Therefore, it is suggested that the BCU does not represent the transition of the rift climax to the post-rift succession in the Hammerfest Basin.

The fault activity stopped in the eastern part of the study area during the deposition of S1 and was

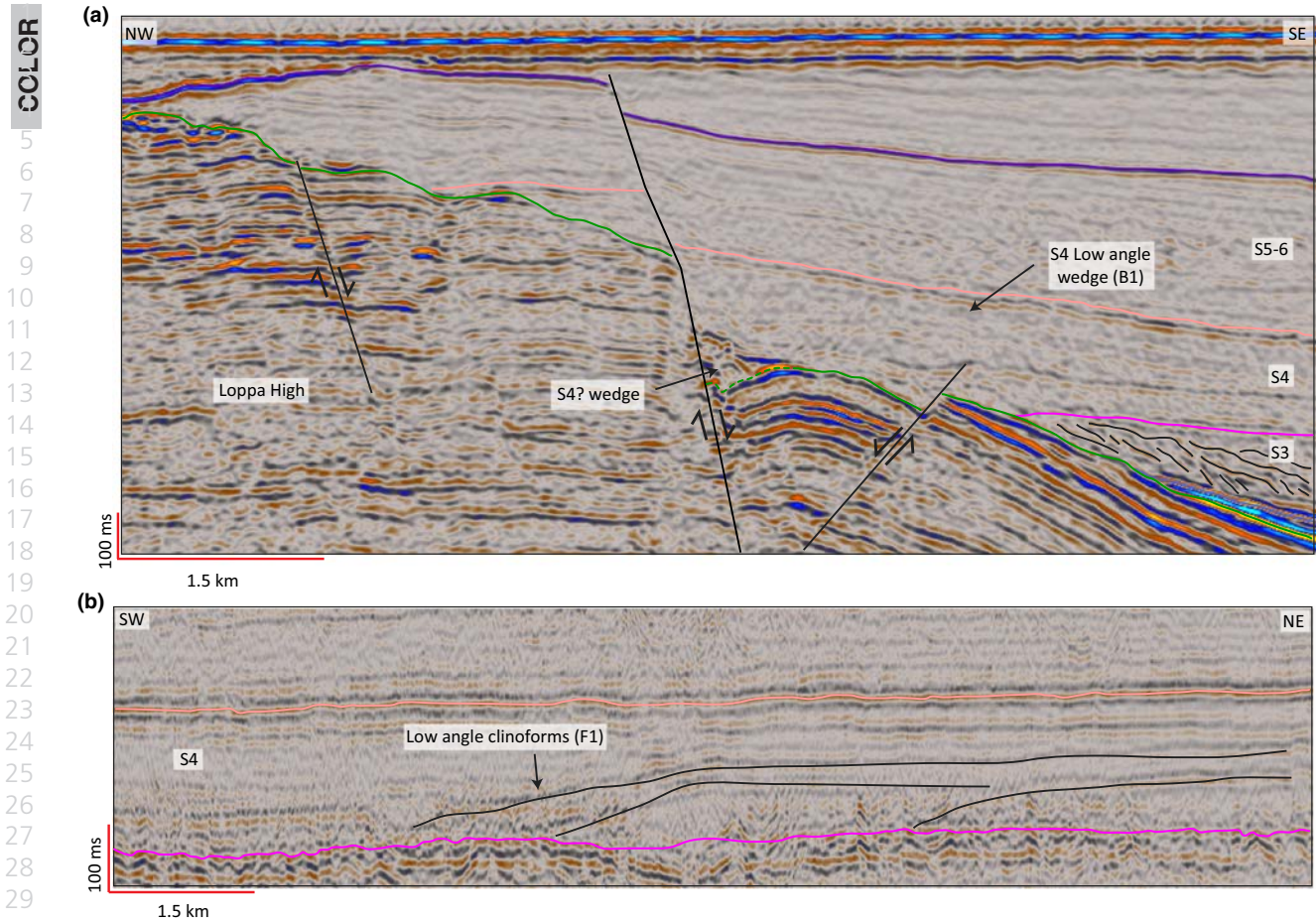


Fig. 11. Seismic lines showing the seismic facies in sequence 4 (SF of S4). (a) Faults in the northern part of the basin and their related wedges (SF B1), note the clinoforms (SF F3) in S3. (b) Low-angle, low-relief clinoforms (SF F1) prograding to the SW in S4. Location of the seismic lines is indicated in Fig. 5a.

concentrated in the western part of the basin until the deposition of S2 (e.g. FF3 and FF2). This is supported by thickness variations, the development of the north-western and the south-eastern depocenters during the deposition of S2 and the deposition of wedges associated with faults (Figs 8c, 7b and 12c). These observations suggest a diachronous transition between the rift climax and the post-rift succession across the Hammerfest Basin similar to the northern North Sea (Gabrielsen *et al.*, 2001; Zachariah *et al.*, 2009).

The nature of the feeder system

Whereas the two previous factors control the distribution of the clastic wedges, the nature of the feeder system controls their geometry and connectivity (Stow *et al.*, 1996). Lateral continuous wedges parallel to the strike of the TFFC are interpreted in the southern part of the basin, as slope deposits fed by a linear source (Figs 9a and 12a). Slope deposits fed by a linear source are characterized by complex depositional

systems (Reading & Richards, 1994; Stow *et al.*, 1996; Galloway, 1998; Gawthorpe & Leeder, 2000; Leppard & Gawthorpe, 2006), which can make facies more difficult to predict. Point sources forming well-defined submarine fans are interpreted in the north-western part of the basin within S2 (Fig. 7a), indicating more predictable facies.

In summary, during the rift climax stage, the geometry, distribution of depositional systems and the input of sediments in a basin are controlled by the interaction of several variables such as: 1) variability along the strike of the main bounding faults (Gawthorpe *et al.*, 1990; Gupta *et al.*, 1998; McLeod *et al.*, 2002; Elliott *et al.*, 2012, 2017, 2017); 2) diachronous movement of the faults; and 3) nature of the feeder system (Reading & Richards, 1994; Stow *et al.*, 1996; Galloway, 1998; Gawthorpe & Leeder, 2000; Leppard & Gawthorpe, 2006). Although variations in footwall lithology are not considered here, this may be an important factor affecting the amount of coarse-grained sediment transported into the basin (McArthur *et al.*, 2013).

COLOR

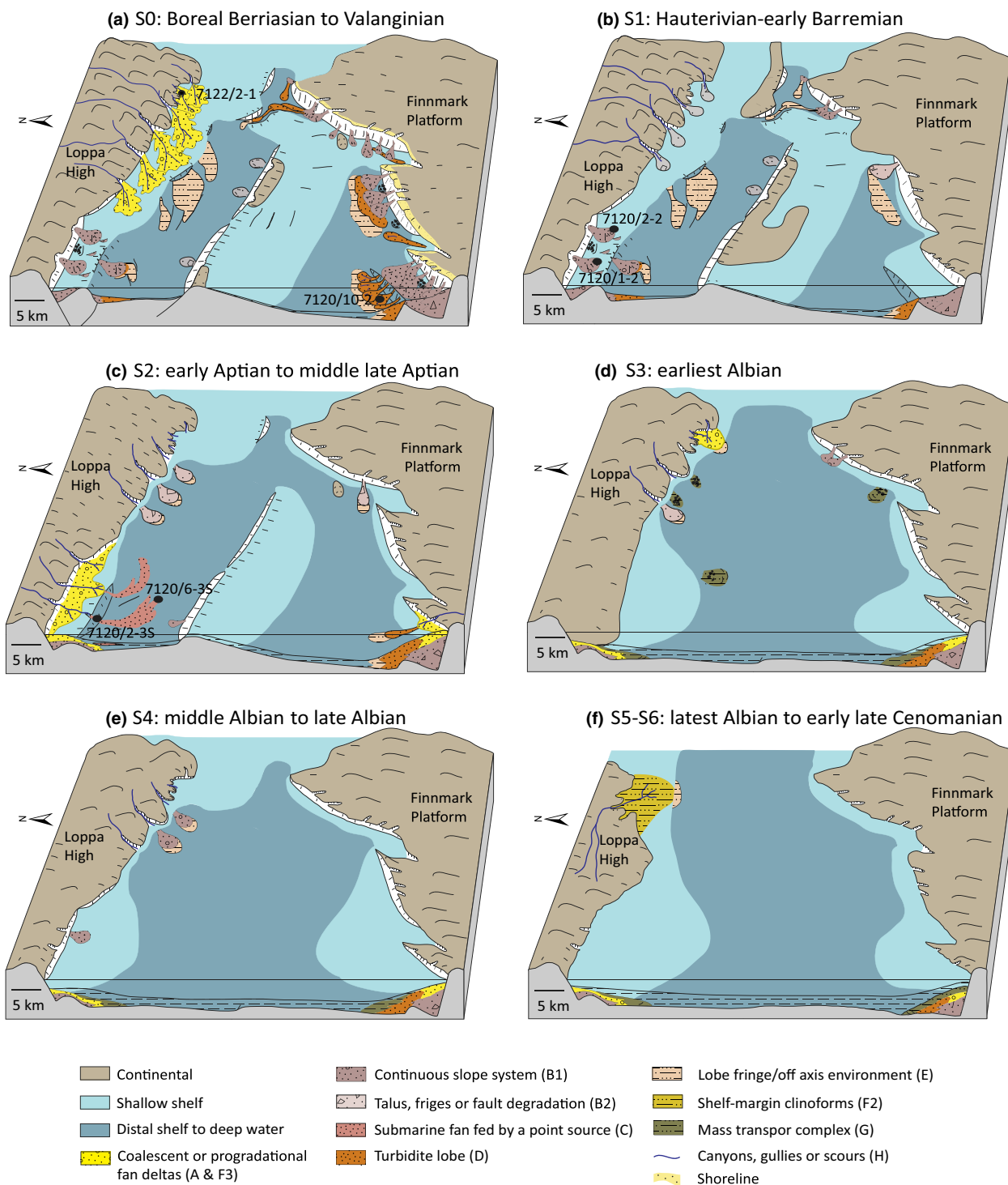


Fig. 12. Three-dimensional palaeogeographic reconstruction of the entire Hammerfest Basin showing the tectosedimentary evolution of the Lower Cretaceous succession. (a) Sequence 0 (Boreal Berriasian/Volgian to Valanginian or younger); (b) Sequence 1 (Hauterivian to early Barremian); (c) Sequence 2 (early Aptian to middle late Aptian); (d) Sequence 3 (earliest Albian); (e) Sequence 4 (middle Albian- late Albian); (f) Sequences 5 and 6 (latest Albian early to late Cenomanian). See the main text for detailed discussion on each sequence and how tectonic activity have controlled the distribution of the sedimentary wedges, submarine fans and clinoforms.

Controls during post-rift

Remnant topography of the basin flanks inherited from the syn-rift stage

The Hammerfest Basin is a symmetric feature characterized by two main uplifted flanks: the Finnmark Platform and the Loppa High (Fig. 2). At the time of the deposition of S3, a relatively homogeneous topography is interpreted based on the time thickness maps (Fig. 8), where the influence of the central high was no longer evident. The remnant topography inherited from the syn-rift period is not a major factor that influenced the input of coarse-grained sediment to the basin. Only localized areas of the Finnmark Platform provided sediment to a prograding shoreline/fan delta (wedges B1; Fig. 10a). The topography of the Loppa High during the post-rift was conditioned by fault activity in its western flank (Faleide *et al.*, 1993; Indrevær *et al.*, 2016), rather than inherited from the main syn-rift period of the Hammerfest Basin. This contrasts to areas as the northern North Sea, where uplifted and rotated fault blocks developed within the syn-rift period were a major factor affecting the post-rift deposition (Nøttvedt *et al.*, 1995; Zachariah *et al.*, 2009).

Local reactivation of faults

Preferential reactivation of fault condition the input of sediments in a basin. In the Hammerfest Basin, the presence of wedges related to the AFC indicates a local reactivation of this fault complex in the northern boundary with the Loppa High (Fig. 11a). This resulted in localized depocenters with associated wedges in the adjacent hangingwalls of the reactivated faults within S4.

Rifting in the adjacent basins

In the study area, fault activity in the eastern part of the Tromsø Basin renewed the topography of the western Loppa High during the Aptian–Albian (Faleide *et al.*, 1993), and uplifted and tilted the Hammerfest Basin eastwards. This event triggered a larger drainage system in the Loppa High, directed away from the Tromsø Basin towards a gentler slope. Therefore, sediment was sourced from the western part of the Loppa High and deposited in the north-eastern Hammerfest Basin as clinoforms identified within S3 and S5–S6 (Fig. 6a).

Rifting in adjacent basins can contribute to the input of potential coarse-grained sediment to a basin even in periods of high eustatic sea level. In the study area, the mid-Cretaceous eustatic sea-level rise (Haq, 2014) and differential subsidence resulted in flooding of some of the structural highs (e.g. the eastern part of the Loppa High), affecting the sedimentation during the

Albian–Cenomanian (S4–S6). Development of clastic wedges was mainly recognized in the areas affected by far field tectonic influence, which overcomes the relative sea level. In other areas of the basin, the continuous to semi-continuous reflectors with medium amplitude reflect that mainly mud from an open-marine environment (Mørk *et al.*, 1999) was deposited in the post-rift succession. The observations presented here suggest that rifting in adjacent basins is an important factor controlling the renewed topography, which triggers preferential sources of sediment.

In summary, during the post-rift stage, the topography in a basin and the depositional system distribution are controlled by the following variables: 1) rifting in adjacent basins; 2) remnant topography of the basin flanks inherited from the syn-rift period (Prosser, 1993; Nøttvedt *et al.*, 1995; Zachariah *et al.*, 2009); and 3) local reactivation of faults.

Many of the depositional systems and geometries described in this article coincide with the previous tectonostratigraphic models for marine rift systems (Gawthorpe & Leeder, 2000). However, these previous models do not explain variables such as the preferential input of sediment in parts of the basin. We suggest that the tectonostratigraphic models for rift basins should be updated, considering a more regional scale and integrating information of neighbouring basins. As a result, variables such as the influence of adjacent rift systems and diachronous movement of the faults, extensively described in both aborted and break-up rift systems (e.g. Rabinowitz & Labrecque, 1979; Gabrielsen *et al.*, 2001; Mohriak & Leroy, 2013), can be included in these tectonostratigraphic models.

CONCLUSIONS

Twelve seismic facies, which represent shallow to deep-marine depositional environments in proximal to distal positions to the main bounding faults, are interpreted based on seismic data, well ties and sedimentological core descriptions. The rift climax in the Hammerfest Basin occurred mainly during the Volgian–Barremian, but the transition to the post-rift succession is diachronous, being younger towards the western part of the basin. The evolution of the post-rift succession in the basin was controlled by three main factors: the influence of an adjacent rift event, the remnant topography of the Finnmark Platform and the local reactivation of faults.

We recognize four main stages in the tectonostratigraphic evolution of the Hammerfest Basin: 1) the Boreal Berriasian/Volgian–Barremian stage, where a fully linked fault array controlled the coarse-grained deposition of S0 and S1 in the area, and fan deltas or shorelines formed in the north, and a laterally continuous, sand-dominated



slope system developed in the south. Shallow marine to continental environments is suggested in the north, east and central parts of the basin, whereas deep-marine environments are interpreted in the south-western part; 2) during the Aptian stage, the input of coarse-grained sediments of S2 was preferential in the north-western and south-western corners of the basin, which is the result of the tectonic activity of the western Asterias Fault Complex and Troms-Finnmark Fault Complex, and renewed topography in the western Loppa High associated with fault activity in the Tromsø Basin; 3) in the Albian stage, remnant topography provided sediments for fan delta/shoreline progradations recorded in S3-S4. Local fault activity in the northern part of the basin controlled the deposition of footwall wedges in S4. Furthermore, a shift in the depocenters from the western part in S0-S2 to the eastern part in S3-S6 reflect a shallower environment in the westernmost part of the Hammerfest Basin; 4) during the latest Albian-Cenomanian stage, the south-eastern Loppa High was flooded due to a combination of an eustatic sea-level rise and local tectonism, but the western part remained a high, providing sediments to allow shelf-margin progradation.

We conclude that tectonostratigraphic models for rift basins should be revised considering a regional scale, where variables such as rifting in adjacent basins can be incorporated. These updated models could explain renewed topography and preferential input of sediments in a basin during the post-rift stage.

ACKNOWLEDGEMENTS

This study is part of the industry-sponsored LoCrA consortium. We acknowledge them for their financial support. We acknowledge Atle Rotevatn, Gijs Henstra, Anna Pontén and Gavin Elliot for their constructive comments and suggestions on the manuscript. We are also grateful to Harald Brunstad for allowing us to use the sedimentological log of well 7122/2-1 and to Ichron Ltd. for providing the logs of wells 7120/2-2, 7120/1-2, 7120/2-3S and 71206-3S. We thank Eni Norge AS for allowing us to use the internal report of well 7120/10-2. We also thank the Norwegian DISKOS database permission to use information from two and three-dimensional seismic and well data. In addition, we thank Lundin Norway AS and PGS for permission to use the information of two three-dimensional seismic cubes and also thanks to Halliburton-Landmark for the software provided. S.-A. Grundvåg also received funding from the ARCEX project (Research Centre for Arctic Petroleum Exploration), which is funded by the Research Council of Norway (grant number 228107). KKS acknowledges Charlotte Olsen (GEUS) and Annette Ryge (GEUS) for palynological slides preparation

and the Norwegian Petroleum Directorate (NPD) for providing palynological slides from well 7121/5-2.

REFERENCES

- AHMED, W. (2012) Structural Analysis of the Troms-Finnmark Fault Complex, SW Barents Sea. Master thesis, University of Oslo, 143.
- ALLEN, P.A. & DENSMORE, A. (2000) Sediment flux from an uplifting fault block. *Basin Res.*, **12**, 367-380.
- APTEC (2007) Well 7120/10-2: Palynological analysis of core samples. Internal Report, Eni Norge AS.
- ÅRHUS, N., KELLY, S.R., COLLINS, J.S. & SANDY, M.R. (1990) Systematic palaeontology and biostratigraphy of two early cretaceous condensed sections from the Barents Sea. *Polar Res.*, **8**, 165-194.
- BAILEY, D. & BioStrat (2017). Early and Late Cretaceous zonation. Retrieved from <http://www.biostrat.org.uk/index.html#>
- BERGLUND, L., AUGUSTSON, J., FÆRSETH, R., GJELBERG, J. & RAMBERG-MOE, H. (1986) The evolution of the hammerfest basin. In: *Habitat of Hydrocarbons on the Norwegian Continental Shelf* (Ed. by Spencer A.M.) *Norwegian Pet. Soc. Graham Trotman*, ????, 319-338.
- CARTWRIGHT, J. (2011) Diagenetically induced shear failure of fine-grained sediment and the development of polygonal fault systems. *Mar. Pet. Geol.*, **28**, 1593-1610.
- CLARK, S., GLORSTAD-CLARK, E., FALEIDE, J., SCHMID, D., HARTZ, E. & FJELDSKAAR, W. (2014) Southwest barents sea rift basin evolution: comparing results from backstripping and time-forward modelling. *Basin Res.*, **26**, 550-566.
- COWIE, P., GUPTA, S. & DAWERS, N. (2000) Implications of fault array evolution for synrift depocentre development: insights from a numerical fault growth model. *Basin Res.*, **12**, 241-261.
- DABRIO, C. (1990) Fan-delta facies associations in late neogene and quaternary basins of Southeastern Spain. In: *Coarse-Grained Deltas* (Ed. by Colella A. & Prior D.B.) *Spec. Publ. Int. Ass. Sediment*, ????, 91-111.
- DALLAND, A., WORSLEY, D. & OFSTAD, K. (1988) A lithostratigraphic scheme for the Mesozoic and cenozoic succession offshore Norway North of 62 N. *Norw. Petrol. Direct. Bull.*, **4**, 67.
- DEIBERT, J.E., BENDA, T., LOSETH, T., SCHELLPEPER, M. & STEEL, R.J. (2003) Eocene clinoform growth in front of a storm-wave-dominated shelf, central basin, Spitsbergen: no significant sand delivery to deepwater areas. *J. Sediment. Res.*, **73**, 546-558.
- DORÉ, A.G. (1991) The structural foundation and evolution of Mesozoic seaways between Europe and the arctic. *Palaeogeogr. Palaeoclimatol. Palaeoecol.*, **87**, 441-492.
- ELLIOTT, G.M., WILSON, P., JACKSON, C.A.L., GAWTHORPE, R.L., MICHELSEN, L. & SHARP, I.R. (2012) The linkage between fault throw and footwall scarp erosion patterns: an example from the bremstein fault complex, offshore Mid-Norway. *Basin Res.*, **24**, 180-197.
- ELLIOTT, G.M., JACKSON, C.A.L., GAWTHORPE, R.L., WILSON, P., SHARP, I.R. & MICHELSEN, L. (2017) Late syn-rift evolution of the vingleia fault complex, Halten Terrace, offshore

- 1 Mid-Norway; a test of rift basin tectono-stratigraphic models.
2 *Basin Res.*, **29**, 465–487.
- 3 FALDEIDE, J.I., VÅGNES, E. & GUDLAUGSSON, S.T. (1993) Late
4 Mesozoic-Cenozoic evolution of the South-Western barents
5 sea in a regional rift-shear tectonic setting. *Mar. Pet. Geol.*,
6 **10**, 186–214.
- 7 FREY, R.W. & PEMBERTON, S.G. (1985) Biogenic structures in
8 outcrops and cores. I. Approaches to ichnology. *Bull. Can.*
9 *Pet. Geol.*, **33**, 72–115.
- 10 GABRIELSEN, R.H., FAERSETH, R.B., JENSEN, L.N., KALHEIM,
11 J.E. & RISS, F. (1990) Structural elements of the Norwegian
12 Continental Shelf. Pt. 1. The barents sea region. *Norw. Petrol.*
13 *Direct. Bull.*, **6**, 47.
- 14 GABRIELSEN, R.H., KYRKJEBØ, R., FALDEIDE, J.I., FJELDSKAAR, W.
15 & KJENNERUD, T. (2001) The cretaceous post-rift basin con-
16 figuration of the Northern North Sea. *Petrol. Geosci.*, **7**, 137–
17 154.
- 18 GALLOWAY, W.E. (1989) Genetic stratigraphic sequences in
19 Basin Analysis I: architecture and genesis of flooding-surface
20 bounded depositional units. *AAPG Bull.*, **73**, 125–142.
- 21 GALLOWAY, W.E. (1998) Siliciclastic slope and base-of-slope
22 depositional systems: component facies, stratigraphic archi-
23 tecture, and classification. *AAPG Bull.*, **82**, 569–595.
- 24 GAWTHORPE, R. & LEEDER, M. (2000) Tectono-sedimentary evo-
25 lution of active extensional basins. *Basin Res.*, **12**, 195–218.
- 26 GAWTHORPE, R., HURST, J. & SLADEN, C. (1990) Evolution of
27 miocene footwall-derived coarse-grained deltas, gulf of suez,
28 Egypt: implications for exploration (1). *AAPG Bull.*, **74**,
29 1077–1086.
- 30 GAWTHORPE, R.L., SHARP, I., UNDERHILL, J.R. & GUPTA, S.
31 (1997) Linked sequence stratigraphic and structural evolution
32 of propagating normal faults. *Geology*, **25**, 795–798.
- 33 GLORSTAD-CLARK, E. (2011) Basin Analysis in the Western Bar-
34 ents Sea Area: The Interplay between Accommodation Space
35 and Depositional Systems. PhD thesis, University of Oslo,
36 212.
- 37 GRUNDVÅG, S.-A., JOHANNESSEN, E.P., HELLAND-HANSEN, W. &
38 PLINK-BJÖRKLUND, P. (2014) Depositional architecture and
39 evolution of progradationally stacked lobe complexes in the
40 Eocene central basin of Spitsbergen. *Sedimentology*, **61**, 535–
41 569.
- 42 GRUNDVÅG, S.A., MARIN, D., KAIRANOV, B., ŚLIWIŃSKA, K.K.,
43 NØHR-HANSEN, H., JELBY, M.E., ESCALONA, A. & OLAUSSEN,
44 S. (2017) The lower cretaceous succession of the Northwest-
45 ern barents shelf: onshore and offshore correlations. *Mar. Pet.*
46 *Geol.*, **86**, 834–857.
- 47 GUPTA, S., COWIE, P.A., DAWERS, N.H. & UNDERHILL, J.R.
48 (1998) A mechanism to explain rift-basin subsidence and
49 stratigraphic patterns through fault-array evolution. *Geology*,
50 **26**, 595–598.
- 51 HAQ, B.U. (2014) Cretaceous eustasy revisited. *Global Planet.*
52 *Change*, **113**, 44–58.
- 53 HELLAND-HANSEN, W. & HAMPSON, G.J. (2009) Trajectory anal-
54 ysis: concepts and applications. *Basin Res.*, **21**, 454–483.
- 55 HENSTRA, G.A., GRUNDVÅG, S.-A., JOHANNESSEN, E.P., KRIS-
TENSEN, T.B., MIDTKANDAL, I., NYSTUEN, J.P., ROTEVATN, A.,
SURLYK, F., SÆTHER, T. & WINDELSTAD, J. (2016) Deposi-
tional processes and stratigraphic architecture within a coarse-
grained rift-margin turbidite system: the Wollaston Forland
Group, East Greenland. *Mar. Pet. Geol.*, **76**, 187–209.
- HENSTRA, G.A., GAWTHORPE, R.L., HELLAND-HANSEN, W.,
RAVNÅS, R. & ROTEVATN, A. (2017) Depositional systems in
multiphase rifts: seismic case study from the Lofoten Margin,
Norway. *Basin Res.*, **29**, 447–469.
- INDREVÆR, K., GABRIELSEN, R.H. & FALDEIDE, J.I. (2016) Early
cretaceous synrift uplift and tectonic inversion in the loppa
high area, Southwestern Barents Sea, Norwegian Shelf. *J.*
Geol. Soc., **171**, 6–2066.
- JACQUIN, T., DARDEAU, G., DURLET, C., DE GRACIANSKY, P.-
C. & HANTZPERGUE, P. (1998) The North sea cycle: an
overview of 2nd-order transgressive/regressive facies cycles
in Western Europe. In: *Mesozoic and Cenozoic Sequence*
Stratigraphy of European Basins (Ed. by de Graciansky
P.C., Hardenbol J., Jaquin T. & Vail P.R.) *SEPM Spec.*
Publ., **60**, 397–409.
- JAKOBSSON, M., MAYER, L., COAKLEY, B., DOWDESWELL, J.A.,
FORBES, S., FRIDMAN, B., HODNESDAL, H., NOORMETS, R.,
PEDERSEN, R. & REBESCO, M. (2012) The international bathy-
metric chart of the Arctic Ocean (Ibco) Version 3.0. *Geophys.*
Res. Lett., **39**, ???–???.
- KNELLER, B. (1995) Beyond the turbidite paradigm: physical
models for deposition of turbidites and their implications for
reservoir prediction. In: *Characterization of Deep Marine Clastic*
Systems (Ed. by Hartley A.J. & Prosser D.J.) *Geol. Soc.*
Spec. Publ., **94**, 31–49, London.
- KNUTSEN, S.-M., AUGUSTSON, J.H. & HAREMO, P. (2000)
Exploring the Norwegian part of the Barents Sea—Norsk
Hydro's Lessons from Nearly 20 years of experience. In:
Improving the Exploration Process by Learning From the Past,
Proceedings of the Norwegian Petroleum Society Conference (Ed.
by Ofstad K., Kittilsen J.E. & Alexander-Marrack P.) *Norve-*
gian Pet. Soc. Spec. Publ., **9**, 99–112.
- LARSEN, M., RASMUSSEN, T. & HJELM, L. (2010). Cretaceous
revisited: exploring the syn-rift play of the faroe-shetland
basin. In: *Petroleum Geology; From Mature Basins to new Fron-*
tiers; Proceedings of the 7th Petroleum Geology Conference (Ed.
by Vining B.A. & Pickering S.C.) *Geol. Soc. Lond.*, **7**, 953–
962.
- LARSEN, G., ELVEBAKK, G., HENRIKSEN, L.B., KRISTENSEN, S.,
NILSSON, I., SAMUELSBERG, T., SVANÅ, T., STEMMERIK, L. &
WORSLEY, D. (2002) Upper palaeozoic lithostratigraphy of the
Southern Norwegian barents sea. *Norw. Petrol. Direct. Bull.*,
9, 76.
- LEKNES, L. (2008) 2D Modelling of the Cenozoic evolution in
the southwestern Barents Sea- with focus on the Pliocene and
the Pleistocene glacial erosion. Master thesis, University of
Stavanger, 86.
- LEPPARD, C.W. & GAWTHORPE, R.L. (2006) Sedimentology of
rift climax deep water systems; lower rudeis formation, ham-
mam faraun fault block, Suez Rift, Egypt. *Sed. Geol.*, **191**, 67–
87.
- LOWE, D.R. (1982) Sediment gravity flows; II, Depositional
models with special reference to the deposits of high-density
turbidity currents. *J. Sediment. Res.*, **52**, 279–297.
- LUNDIN, E. & DORÉ, A. (1997) A tectonic model for the
norwegian passive margin with implications for the NE

- Atlantic: early cretaceous to break-up. *J. Geol. Soc.*, **154**, 545–550.
- MARÍN, D., ESCALONA, A., ŚLIWIŃSKA, K.K., NÖHR-HANSEN, H. & MORDASOVA, A. (2017) Sequence stratigraphy and lateral variability of lower cretaceous clinofolds in the Southwestern Barents Sea. *AAPG Bull.*, **101**, 1487–1517.
- McARTHUR, A.D., HARTLEY, A.J. & JOLLEY, D.W. (2013) Stratigraphic development of an Upper Jurassic Deep Marine Syn-Rift Succession, Inner Moray Firth Basin, Scotland. *Basin Res.*, **25**, 285–309.
- McLEOD, A.E., UNDERHILL, J.R., DAVIES, S.J. & DAWERS, N.H. (2002) The influence of fault array evolution on synrift sedimentation patterns: controls on deposition in the Strathspey–Brent–Statfjord Half Graben, Northern North Sea. *AAPG Bull.*, **86**, 1061–1094.
- MOHRIAK, W.U. & LEROY, S. (2013) Architecture of rifted continental margins and break-up evolution: Insights from the South Atlantic, North Atlantic and Red Sea–Gulf of Aden Conjugate Margins. *Geol. Soc. Lond. Spec. Publ.*, **369**, 497–535.
- MORK, A., DALLMANN, W., DYPVIK, H., JOHANNESSEN, E., LARSEN, G., NAGY, J., NÖTTVEDT, A., OLAUSSEN, S., PHELINA, T. & WORSLEY, D. (1999) Mesozoic lithostratigraphy. In: *Lithostratigraphic Lexicon of Svalbard. Upper Palaeozoic to Quaternary Bedrock. Review and Recommendations for Nomenclature use* (Ed. by W.K. Dallmann), pp. 127–214. Norwegian Polar Institute, Tromsø.
- MOSCARDELLI, L. & WOOD, L. (2008) New classification system for mass transport complexes in offshore trinidad. *Basin Res.*, **20**, 73–98.
- MULDER, T. & ALEXANDER, J. (2001) The physical character of subaqueous sedimentary density flows and their deposits. *Sedimentology*, **48**, 269–299.
- NÖHR-HANSEN, H. (1993) Dinoflagellate cyst stratigraphy of the Barremian to Albian, Lower Cretaceous, East Greenland. *Bull. Grøn. Geol. Unders.*, **166**, 171.
- NÖHR-HANSEN, H. (2012) Palynostratigraphy of the cretaceous–lower palaeogene sedimentary succession in the Kangerlussuaq Basin, Southern East Greenland. *Rev. Palaeobot. Palynol.*, **178**, 59–90.
- NORMARK, W.R. (1978) Fan valleys, channels, and depositional lobes on modern submarine fans: characters for recognition of sandy turbidite environments. *AAPG Bull.*, **62**, 912–931.
- NÖTTVEDT, A., GABRIELSEN, R. & STEEL, R. (1995) Tectonostratigraphy and sedimentary architecture of rift basins, with reference to the Northern North Sea. *Mar. Pet. Geol.*, **12**, 881–901.
- NPD (2017) Norwegian Petroleum Directorate Factpages. <http://factpages.npd.no/factpages/Default.aspx?culture=en> (Accessed January 2017).
- PRÉLAT, A., HODGSON, D.M. & FLINT, S.S. (2009) Evolution, architecture and hierarchy of distributary deep-water deposits: a high-resolution outcrop investigation from the Permian Karoo Basin, South Africa. *Sedimentology*, **56**, 2132–2154.
- PROSSER, S. (1993) Rift-related linked depositional systems and their seismic expression. In: *Tectonics and Seismic Sequence Stratigraphy* (Ed. by Williams G.D. & Dobb A.) *Geol. Soc. Lond. Spec. Publ.*, **71**, 35–66.
- RABINOWITZ, P.D. & LABRECQUE, J. (1979) The Mesozoic South Atlantic ocean and evolution of its continental margins. *J. Geophys. Res. Solid Earth*, **84**, 5973–6002.
- RAVNÅS, R. & STEEL, R.J. (1998) Architecture of marine rift-basin successions. *AAPG Bull.*, **82**, 110–146.
- READING, H. & COLLINSON, J. (1996) Clastic coasts. In: *Sedimentary Environments: Processes, Facies and Stratigraphy*, 3rd edn (Ed. by H.G. Reading), pp. 154–231. Blackwell Scientific Publications, Oxford.
- READING, H.G. & RICHARDS, M. (1994) Turbidite systems in deep-water basin margins classified by grain size and feeder system. *AAPG Bull.*, **78**, 792–822.
- SALAZAR, M., MOSCARDELLI, L. & WOOD, L. (2015) Utilising clinofold architecture to understand the drivers of basin margin evolution: a case study in the Taranaki Basin, New Zealand. *Basin Res.*, <https://doi.org/10.1111/bre.12138>.
- SANCHEZ, C.M., FULTHORPE, C.S. & STEEL, R.J. (2012) Miocene shelf-edge deltas and their impact on deepwater slope progradation and morphology, Northwest Shelf of Australia. *Basin Res.*, **24**, 683–698.
- SANDVIK, S. (2014) Description and Comparison of Lower Cretaceous Deposits from Svalbard and the Southern Loppa High. Master thesis, University of Bergen, 135.
- SATTAR, N. (2008) Mapping of Lower Cretaceous (Knurr Sandstone) Turbidite Lobes Using Seismic Stratigraphy and Prospectivity Along the Southern Loppa High Margin, Hammerfest Basin, Barents Sea, Norway. Master thesis, University of Uppsala, 85.
- SELDAL, J. (2005) Lower cretaceous: the next target for oil exploration in the barents sea? In: *Petroleum Geology: North-West Europe and Global Perspectives – Proceedings of the 6th Petroleum Geology Conference* (Ed. by Doré A.G. & Vining B.A.) *Geol. Soc. Lond.*, **6**, 231–240.
- SHANMUGAM, G. & MOIOLA, R. (1991) Types of submarine fan lobes: models and implications (1). *AAPG Bull.*, **75**, 156–179.
- SNEIDER, J.S., DE CLARENS, P. & VAIL, P.R. (1995) Sequence stratigraphy of the middle to Upper Jurassic, Viking Graben, North Sea. In: *Sequence Stratigraphy on the Northwest European Margin* (Ed. by Steel R.J., Felt V.L., Johannessen E.P. & Mathieu C.) *Norwegian Pet. Soc. Spec. Publ.*, **5**, 167–197.
- SØMME, T.O., JACKSON, C.A.L. & VAKSDAL, M. (2013) Source-to-sink analysis of ancient sedimentary systems using a subsurface case study from the Møre-Trøndelag Area of Southern Norway: part 1—depositional setting and fan evolution. *Basin Res.*, **25**, 489–511.
- STEEL, R.J., CARVAJAL, C., PETTER, A.L. & UROZA, C. (2008) Shelf and shelf-margin growth in scenarios of rising and falling sea level. *Recent Adv. Mod. Siliciclastic Shallow-Marine Stratigr. SEPM, Spec. Publ.*, **90**, 47–71.
- STOW, D.A.V., READING, H.G. & COLLINSON, J.D. (1996) Deep seas. In: *Sedimentary Environments: Processes, Facies and Stratigraphy*, 3rd edn (Ed. by H.G. Reading), pp. 395–454. Blackwell Scientific Publications, Oxford.
- SUND, T., SKARPNES, O., JENSEN, L.N. & LARSEN, R. (1986) Tectonic development and hydrocarbon potential offshore Troms, Northern Norway. In: *Future Petroleum Provinces*

- 1 of the World (Ed. by Halbouty M.T.) *AAPG Mem.*, **40**,
2 615–627.
- 3 SURLYK, F. (1978) Submarine fan sedimentation along fault
4 scarps on tilted fault blocks. *Bull. Grøn. Geol. Unders.*, **128**,
5 1–108.
- 6 SURLYK, F. (1989) Mid-Mesozoic syn-rift turbidite systems:
7 controls and predictions. In: *Correlation in Hydrocarbon*
8 *Exploration* (Ed. By Collinson J.D.) *Norwegian Pet. Soc. Gra-*
9 *ham Trotman Lond.*, ????, 231–241.
- 10 WALKER, R.G. (1978) Deep-water sandstone facies and ancient
11 submarine fans: models for exploration for stratigraphic traps.
12 *AAPG Bull.*, **62**, 932–966.
- 13 WILLIAMS, G., BRINKHUIS, H., PEARCE, M., FENSOME, R. & WEE-
14 GINK, J. (2004) Southern Ocean and global dinoflagellate cyst
15 events compared: index events for the Late Cretaceous–Neo-
16 gene. In: *Proceedings of the Ocean Drilling Program, Scientific*
17 *Results* (Ed. by N.F. Exxon, J.P. Kennett, & M.J. Malone),
18 189, pp. 1–98. Available from World Wide Web: [http://](http://www-odp.tamu.edu/publications/189_SR/VOLUME/CHAPTERS/107.PDF)
19 [www-odp.tamu.edu/publications/189_SR/VOLUME/](http://www-odp.tamu.edu/publications/189_SR/VOLUME/CHAPTERS/107.PDF)
20 [CHAPTERS/107.PDF](http://www-odp.tamu.edu/publications/189_SR/VOLUME/CHAPTERS/107.PDF)
- 21 WOOD, R., EDRICH, S. & HUTCHISON, I. (1989) Influence of
22 North Atlantic tectonics on the large-scale uplift of the stape-
23 pen high and loppa high, Western barents shelf: Chapter 36:
24 North Sea and barents shelf. In: *Extensional Tectonics and*
25 *Stratigraphy of the North Atlantic Margins* (Ed. by Tankard
26 A.J. & Balkwill H.R.) *AAPG Mem.*, **46**, 559–566.
- 27 ZACHARIAH, A.J., GAWTHORPE, R., DREYER, T. & CORFIELD, S.
28 (2009) Controls on early post-rift physiography and stratigra-
29 phy, lower to mid-cretaceous, North Viking Graben, Norwe-
30 gian North Sea. *Basin Res.*, **21**, 189–208.

31 *Manuscript received 28 March 2017; In revised form 12*
32 *September 2017; Manuscript accepted 13 September 2017.*